UNIVERSITY OF CALIFORNIA,
IRVINE

Low-Mass Satellite Quenching in The Local Group

DISSERTATION

submitted in partial satisfaction of the requirements
for the degree of

DOCTOR OF PHILOSOPHY

in Physics

by

Sean Philip Fillingham

Dissertation Committee:
Professor Michael C. Cooper, Chair
Professor James S. Bullock
Professor Manoj Kaplinghat

2019

DEDICATION

To Jacquelyn and Olivia

TABLE OF CONTENTS

LIST OF FIGURES

LIST OF TABLES

ACKNOWLEDGMENTS

I would like to thank my family, friends, collegues, and cats for their immense support throughout this process.

(You must acknowledge grants and other funding assistance.

You may also acknowledge the contributions of professors and friends.

You also need to acknowledge any publishers of your previous work who have given you permission to incorporate that work into your dissertation. See Section 3.2 of the UCI Thesis and Dissertation Manual.)

CURRICULUM VITAE

Sean Philip Fillingham

EDUCATION

Doctor of Philosophy in Physics **2019**
University of California, Irvine *Irvine, CA*

Master of Science in Physics **2015**
University of California, Irvine *Irvine, CA*

Bachelor of Science in Physics **2013**
University of California, Los Angeles *Los Angeles, CA*

RESEARCH EXPERIENCE

Graduate Research Assistant **2014–2019**
University of California, Irvine *Irvine, California*

Undergraduate Research Assistant **2012–2013**
University of California, Los Angeles *Los Angeles, California*

TEACHING EXPERIENCE

Teaching Assistant **2013–2015**
University of California, Irvine *Irvine, California*

REFEREED JOURNAL PUBLICATIONS

Taking Care of Business in a Flash ϟ: Constraining the Timescale for Low-Mass Satellite Quenching with ELVIS **2015**
MNRAS

Under Pressure: Quenching Star Formation in Low-Mass Satellite Galaxies via Stripping **2016**
MNRAS

Environmental Quenching of Low-Mass Field Galaxies **2018**
MNRAS

Gaia Quenching **2019**
submitted to MNRAS

ABSTRACT OF THE DISSERTATION

Low-Mass Satellite Quenching in The Local Group

By

Sean Philip Fillingham

Doctor of Philosophy in Physics

University of California, Irvine, 2019

Professor Michael C. Cooper, Chair

The abstract of your contribution goes here.

Chapter 1

Introduction

Awesome introduction...astrophysics is cool!

Chapter 2

Taking Care of Business in a Flash ϟ: Constraining the Timescale for Low-Mass Satellite Quenching with ELVIS

2.1 Introduction

Foremost among the results of galaxy surveys over the last decade has been the realization that the galaxy population at $z \lesssim 2$ is bimodal in nature [e.g. **?** **?** **?** **?**]. That is, galaxies both locally and out to intermediate redshift are effectively described as one of two distinct types: red, early-type galaxies lacking significant star formation and blue, late-type galaxies with active star formation. In color-magnitude space, the red galaxies populate a tight relation (often called the red sequence), while the distribution of blue galaxies is more scattered (sometimes referred to as the blue cloud). While the red and blue populations

comprise approximately equal portions of the cosmic stellar mass budget at $z \sim 1$, galaxies on the red sequence dominate today, following a growth in stellar mass within the red population of roughly a factor of 2 over the past 7 Gyr [**?** **?** **?** **?**]. Despite uncertainty regarding the particular physical process(es) at play, the suppression (or quenching) of star formation in blue galaxies, thereby making them red, is one of the principal drivers of this dramatic growth in the number density of quiescent systems at late cosmic time.

At both low and intermediate redshift, the local environment of a galaxy is known to be well-correlated with the suppression of star formation, such that passive or quiescent galaxies preferentially live in higher-density environments [**?** **?** **?** **?** **?** **?**]. While the stellar mass or surface mass density of a galaxy may be more closely connected to quenching for massive systems [**?** **?** **?**], recent work has shown that environment is likely the dominant driver of quenching at the lowest mass scales [$M_\star < 10^9$ $M_\odot$, **?**]. For example, studies comparing satellite galaxies to isolated field systems of similar stellar mass in the local Universe find that satellites tend to exhibit lower star formation rates, more bulge-dominated morphologies, as well as older and more metal-rich stellar populations [**?** **?** **?** **?** **?** **?**]. This observed suppression of star formation in satellite galaxies is commonly referred to as "environmental quenching". At present, galaxy formation models fail to reproduce this environment-dependent effect in detail, with both semi-analytic and hydrodynamical models overpredicting the number of quenched satellites at low masses [**?** **?** **?** **?** **?**].

Understanding the physics of environmental quenching is complicated by the wide range of physical processes that could be responsible for suppressing star formation in low-mass satellites. For example, various quenching mechanisms preferentially operate on satellite galaxies within overdense environments, including [*i*] "starvation" or "strangulation" – whereby gas accretion onto a satellite galaxy is halted following infall, thus eventually eliminating the fuel for star formation [**?** **?**], [*ii*] "harassment" – by which close encounters between densely packed cluster or group members strip gas from around the interacting galaxies [**?**], and

[*iii*] "ram-pressure stripping" – where the cold dense gas at the center of a satellite (or the hot halo surrounding it) is removed from the galaxy as a result of a high-speed interaction with the hot gas halo of the host [**?** **?**].

To further complicate matters, each of these processes may be important in different host halos and at different satellite mass scales. In an attempt to differentiate between these various physical mechanisms, we aim to measure the timescale upon which satellite quenching occurs across a broad range of satellite stellar mass. Throughout this work, we define this quenching timescale ($\tau_{\rm quench}$) relative to the time at which a satellite was accreted onto its current host system (i.e. relative to the infall time of the satellite). While quenching via starvation will proceed according to the available cold gas reservoir for star formation within an accreted satellite, ram-pressure stripping will largely act on a timescale set by the density distribution of the host's hot halo and infall velocity of the satellite. As such, constraining the timescale for satellite quenching may therefore serve as a critical step towards differentiating between various physical mechanisms.

By comparing satellite samples at low and intermediate redshift to galaxy and dark matter-only simulations, several recent analyses of satellites at high stellar mass ($> 5\times10^9$ M$_\odot$) point towards relatively long quenching timescales of several Gyr or more [**?** **?**]. Remarkably, when pushing this analysis to lower masses ($\sim 10^{8.5} - 10^{9.5}$ M$_\odot$), **?**] find that quenching remains surprisingly inefficient, such that the average quenching timescale increases to > 7 Gyr. Here, we extend these previous analyses of quenching timescales to yet lower masses by studying the satellite galaxies of the Local Group. Through comparison to simulations, we aim to establish a coherent picture of the timescale upon which satellite quenching acts, spanning more than five orders of magnitude in satellite mass. In §2.2, we detail the population of Local Group satellites along with an estimation of the observed quenched fraction. In §2.3 and §2.4, we describe the relevant N-body simulations and physically-motivated quenching models, respectively, detailing the relevant constraints on the derived quenching timescale at

low masses. Finally, in §2.5 and §2.6, we discuss the implications of our analysis, including a "back of the envelope" explanation of the underlying physics operating on low-mass satellites and a summary of our main results.

2.2 Local Group Satellites

In assembling our sample of Milky Way and M31 satellites, we utilize the compilation of local dwarf galaxy properties presented by **?**]. To minimize the potential impact of incompleteness at low masses, we limit our analysis to those dwarfs with measured stellar masses in the range $10^6 - 10^8$ $M_\odot$; however, as discussed in more detail below, including systems at lower masses has very little impact on our qualitative or quantitative results. From this population of local dwarfs, satellite systems are selected to be within 300 kpc of the Milky Way or M31 and bound with respect to their host — i.e. $\sqrt{3} \cdot V_{los} < V_{\rm esc}(r)$, where $V_{\rm esc}(r)$ is the escape velocity at a radial distance of r for an NFW halo with a concentration (c) of 8 and a total halo mass of 2×10^{12} $M_\odot$.[1] To account for potential tangential motion, we multiply all observed line-of-sight velocities from **?**] by a factor of $\sqrt{3}$ in evaluating whether each system is bound. Within the stellar mass range of 10^6 $M_\odot$ to 10^8 $M_\odot$, Figure 2.1 shows the position and velocity of all Local Group dwarfs relative to their host (or nearest massive neighbor in the case of field systems such as the Pegasus dIrr).

We identify 12 satellite systems meeting our selection criteria (see Table 1), with the final set of satellites and corresponding quenched fraction relatively independent of the adopted selection criteria. For instance, field dwarfs such as NGC 6822, Leo T, and Phoenix, which are nearly in our stellar mass limits, are located significantly beyond our radial selection limit (i.e. $>$ 400 kpc from the Milky Way). Moreover, while the observed line-of-sight velocity of Leo I suggests that it may be unbound (see Fig. 2.1), recent proper motion observations

[1] Varying the adopted host halo mass and concentration (and thus our satellite selection limits) does not have a significant effect on our final sample of Local Group satellites.

conclude that the system is very likely bound to the Milky Way even at a distance of more than 250 kpc [**?** **?**]. Finally, given the high metallicity and lack of overdensity in RR Lyrae stars, we categorize Canis Major as an overdensity in the Milky Way and not a satellite [**?** **?** **?** , but see also **?**].

To determine whether a given satellite is quenched, we use the observed HI gas fraction as a proxy for the current star formation rate (SFR), defining dwarfs with atomic gas fractions less than 10% to be quenched (see Fig. 3.2). This criterion leads to only one satellite in our sample, IC 10, categorized as currently star-forming and yields a quenched fraction of $> 90\%$ for satellites bound to the Milky Way and M31 in the selected mass range. Alternative definitions of quenched versus star-forming – e.g. using star-formation histories derived from photometric observations of spatially-resolved stellar populations [**?** **?**] or star-formation rates inferred from Hα emission [**?** **?**] yield similar results. Moreover, our measurement of the satellite quenched fraction is not strongly dependent on the adopted mass range, as the quenched fraction is largely unchanged if we extend the lower mass limit down to 3×10^5 $M_\odot$ so as to account for potential uncertainties or scatter in the stellar mass measurements. Over this expanded stellar mass range, the sample would then also include Leo II, And XXI, And XXV, and LGS 3. While HI measurements suggest that LGS 3 is likely star-forming, a variety of observations, including star formation rates inferred from Hα narrow-band imaging, indicate that Leo II, And XXI, and And XXV are quiescent [**?** **?** **?** **?** **?** **?**]. When including these four lower-mass systems in our sample, the resulting quenched fraction remains quite high ($\sim 87\%$); furthermore, pushing to yet lower masses will similarly yield little variation in the quenched fraction, as the lowest-mass satellites in the Local Group are universally quenched [e.g. **?** **?** **?** **?** **?**].

While our census of satellites in the Local Group is likely incomplete at low masses due to obscuration by or confusion with the disk of both the Milky Way and M31, the focus of our analysis is the relative fraction of star-forming versus quenched systems. Assuming that

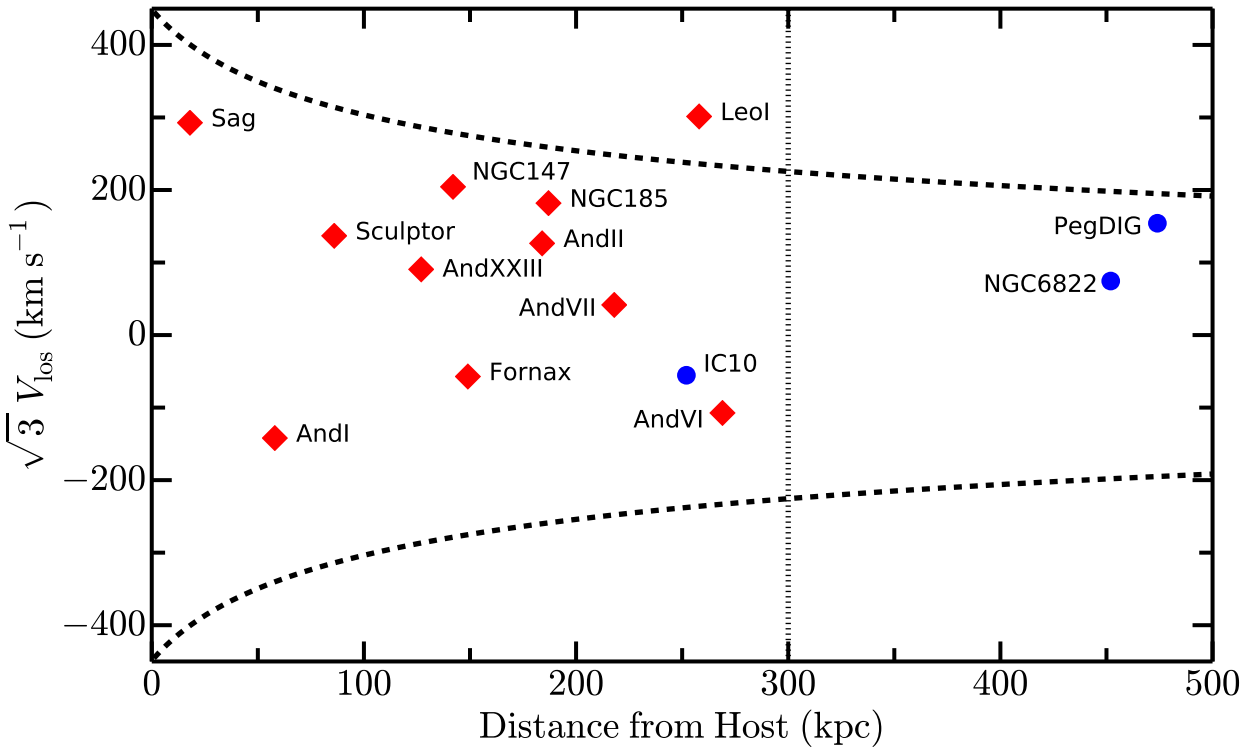

Figure 2.1: Host-centric velocity versus distance for all known Local Group galaxies in the stellar mass range of 10^6–10^8 $M_\odot$. To account for unknown tangential velocities, the observed line-of-sight velocities have been multiplied by a factor of $\sqrt{3}$. The dotted vertical line at 300 kpc corresponds to the expected virial radius of the Milky Way and M31 and represents the radial limit for our satellite selection. The dashed lines show the escape velocity for an NFW halo with a concentration (c) of 8 and a total mass of 2×10^{12} $M_\odot$. Satellites are color-coded as star-forming (blue circles) or quenched (red diamonds) according to their observed HI gas fraction (see Fig. 3.2).

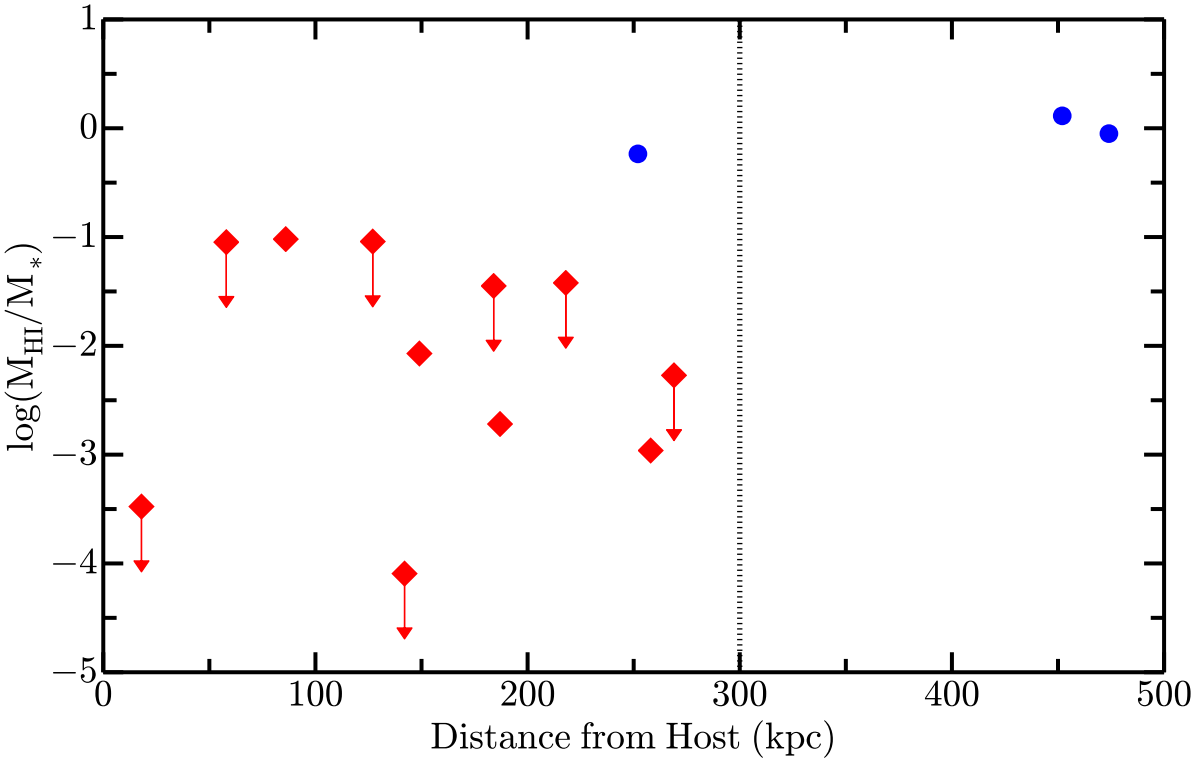

Figure 2.2: Observed HI gas fraction as a function of distance from the nearest host galaxy for local dwarfs included in our mass range of $10^6 - 10^8$ $M_\odot$. Systems with an atomic gas fraction less than 10% are classified as quenched (red diamonds), with more gas-rich dwarfs identified as star-forming (blue circles). At these low masses, roughly 90% of satellites are quenched in the Local Group.

Galaxy Name	Morphology (1)	$M_\star$ (10^6 $M_\odot$) (2)	M_{HI} (10^6 $M_\odot$) (3)	D_{host} (kpc) (4)	V_{los} (km s^{-1}) (5)	Quenched (6)
Milky Way						
Sagittarius	dSph	21	< 0.007	18	169	Yes
Sculptor	dSph	2.3	0.22	86	79	Yes
Fornax	dSph	20	0.17	149	-33	Yes
Leo I	dSph	5.5	< 0.006	258	174	Yes
M31						
And I	dSph	3.9	< 0.35	58	-82	Yes
And XXIII	dSph	1.1	< 0.1	127	52	Yes
NGC 147	dE/dSph	62	< 0.003	142	118	Yes
And II	dSph	7.6	< 0.27	184	73	Yes
NGC 185	dE/dSph	68	0.13	187	105	Yes
And VII	dSph	9.5	< 0.36	218	24	Yes
IC 10	dIrr	86	50	252	-32	No
And VI	dSph	2.8	< 0.015	269	-62	Yes

Table 2.1: Observed properties of satellite galaxies in the Local Group with measured stellar masses in the range $10^6 - 10^8$ $M_\odot$ and located within 300 kpc of either the Milky Way or M31 (separated according to host system): (1) morphological classification and (2) stellar mass from **?**]; (3) atomic gas mass measurements from **?**] and **?**], plus upper limits from the literature [**?** **?** **?** **?**]; (4) distance from the nearest host as given by **?**]; (5) line-of-sight velocity with respect to the host from **?**], with the exception of And XXIII [**?**]; (6) identification as quenched versus star-forming, according to observed atomic gas fraction (see Fig. 3.2).

neither quenched nor star-forming systems preferentially reside in or behind the disk, the quenched fraction should be independent of any such incompleteness. From an analysis of the Palomar and UK Schmidt photographic plates, which cover more than $20,000$ square degrees of sky at high Galactic latitude ($|b| > 20°$), **?**] finds that the known satellite population for the Milky Way is complete down to below our adopted mass limit ($\gtrsim 3 \times 10^5$ $M_\odot$). This conclusion is supported by deeper imaging data from the Sloan Digital Sky Survey [SDSS, **?**], Pan-STARRS [**?**], and Dark Energy Survey [DES, **?**], which cover a significant portion of the northern and southern sky and are complete to beyond the host virial radius (i.e. $>$ 300 kpc) at these stellar masses [**?** **?** **?** **?** **?**].

For M31, our knowledge of satellites is largely based on imaging surveys such as the Pan

Andromeda Archeological Survey [PAndAS, **?** , see also **? ? ?**]. As shown by **?**], PAndAS is complete down to our mass limit within a survey footprint that covers a radial distance of roughly 150 kpc surrounding M31. While recent analysis of imaging data, including that from Pan-STARRS, has likely uncovered several new satellites of M31 at radial distances of $\gtrsim$ 150 kpc [And XXX-XXXIV, **? ? ? ?**], we exclude these systems from our study given that distances (relative to M31) are poorly constrained and potentially greater than 300 kpc. Early analysis of the stellar populations in Andromeda XXXI and XXXII, however, do suggest passive populations devoid of young stars [**?**]. As likely quenched satellites, we note that inclusion of And XXX-XXXIV would have little impact on the observed quenched fraction in the Local Group and thus on the results of our analysis. Moreover, while the M31 satellite population may be incomplete at radial distances of $150 - 300$ kpc from M31, this should have minimal impact on the observed quenched fraction in the Local Group (even assuming that star-forming satellites are possibly biased towards large radial distances, as our results would imply). In §2.4, we discuss this potential selection effect in more detail.

2.3 Simulations

To model the evolution of satellite galaxies in the Local Group, we utilize the Exploring the Local Volume In Simulations (ELVIS) suite of 48 high-resolution, dissipationless simulations of Milky Way-like halos [**?**]. The suite includes 24 isolated halos as well as 12 mass-matched Local Group-like pairs, simulated within high-resolution uncontaminated volumes spanning 2-5 Mpc in size using a particle mass of 1.9×10^5 $M_\odot$ and a Plummer-equivalent force softening of $\epsilon = 141$ physical parsecs. Within the high-resolution volumes, the halo catalogs are complete down to $M_{\rm halo} > 2 \times 10^7$ $M_\odot$, $V_{\rm max} > 8$ km s^{-1}, $M_{\rm peak} > 6 \times 10^7$ $M_\odot$, and $V_{\rm peak} > 12$ km s^{-1} — thus more than sufficient to track the evolution of halos hosting Local Group dwarfs with stellar masses of $> 10^6$ $M_\odot$. ELVIS adopts a cosmological model based

on Wilkinson Microwave Anisotropy Probe 7 [**?**], with the following ΛCDM parameters: $\sigma_8 = 0.801$, $\Omega_m = 0.266$, $\Omega_\Lambda = 0.734$, $n_s = 0.963$, and $h = 0.71$.

As hosts for the Local Group dwarfs in the stellar mass range of $10^6 - 10^8$ $M_\odot$, we select halos in the ELVIS simulations with masses of $M_{peak} = 5 \times 10^9 - 6 \times 10^{10}$ $M_\odot$, following the abundance matching prescription of **?**]. Abundance matching, a common technique for populating simulated dark matter distributions with galaxies, assumes a one-to-one relation between a galaxy's stellar mass and the mass of its parent dark matter (sub)halo [**?** **?**]. While this simple empirical approach to modeling galaxy formation yields great success for massive galaxies, matching a wide range of clustering statistics as a function of cosmic time [e.g. **?** **?**], it potentially breaks down at low masses, where the most massive subhalos of Milky Way-like simulations are inconsistent with the observed dynamics of nearby dwarf galaxies [**?** **?** **?** **?** **?**].

While uncertainties remain in the potential efficacy or robustness of abundance matching prescriptions at low masses, our results are largely unaffected by changes in the assumed stellar mass-halo mass relation. As our fiducial model, we adopt the abundance matching relation of **?**], which in our stellar mass range ($10^6 - 10^8$ $M_\odot$) yields 9 subhalos as candidate satellite hosts within a typical ELVIS parent halo (after removing stripped or disrupted subhalos). When applying the shallower stellar mass-halo mass relation from **?**], the number of potential subhalo hosts increases accordingly, but the quantitative and qualitative results with regard to satellite quenching remain unchanged. To account for potential increased scatter in the abundance matching relation at low masses, we also mimic scatter in the **?**] relation, by broadening the range of halo masses associated with the observed stellar mass range, randomly selecting 9 subhalos within $2 \times 10^9 < M_{peak}/M_\odot < 2 \times 10^{11}$ as satellite hosts. Again, while this biases the subhalo population to lower masses, our results with regard to satellite quenching remain unaffected.

Independent of the particular abundance matching prescription, we account for satellites

that have been tidally-stripped or disrupted — and thus not included in our observational sample — by restricting our analysis to subhalos for which $V_{\rm max}/V_{\rm peak} > 0.3$, where $V_{\rm max}$ is the current ($z = 0$) maximum circular velocity for the halo and $V_{\rm peak}$ is the value of $V_{\rm max}$ when the halo mass is at its maximum. While a halo's maximum halo mass generally occurs prior to infall (typically at $> 1.5\ R_{\rm vir}$), $V_{\rm peak}$ is a good approximation for $V_{\rm infall}$ since a halo's mass, in general, does not change appreciably prior to infall [**?**]. By restricting our analysis to present-day halos with $V_{\rm max}/V_{\rm peak} > 0.3$, we eliminate all subhalos (i.e. satellites) that have lost greater than 90% of their mass since infall, thereby selecting those subhalos that are within the desired mass range and are highly likely to currently host dwarf galaxies (i.e. not disrupted or significantly stripped). Finally, we note that our results are not strongly dependent upon the adopted $V_{\rm max}/V_{\rm peak}$ cut; applying a more conservative selection criterion (e.g. $V_{\rm max}/V_{\rm peak} > 0.5$) does not significantly change our results.

The ELVIS merger trees include 75 snapshots from $z = 125$ to $z = 0$, providing time resolution of roughly 200 Myr. As discussed in more detail in §2.4, we are interested in using ELVIS to explore models where satellite quenching occurs at a fixed physical radius from the host (e.g. within 50 kpc radially). The crossing time on such scales (~ 100 kpc), however, is typically greater than the median time resolution of the snapshots, such that subhalos would potentially pass into and back out of the quenching radius between two successive snapshots. To more precisely determine subhalo orbits within ELVIS, we map the spatial position of each subhalo (relative to its host) at 20 Myr intervals by spline interpolating the position of each subhalo and corresponding host halo across each of the 75 snapshots. This interpolation also allows us to determine the time at which each subhalo was accreted onto its host halo (i.e. the infall time or $t_{\rm infall}$) at greater precision. Due to the linear spacing of the ELVIS snapshots with scale factor (i.e. non-linear spacing with lookback time), the difference in the measured infall time between our interpolated data and that inferred from the standard ELVIS merger trees depends upon the lookback time at which a subhalo is accreted. For systems with $t_{\rm infall} < 3$ Gyr, which place the strongest constraints on the satellite quenching

timescale, the difference in $t_{\rm infall}$ is relatively modest, with a median offset of less than 0.5 Gyr for our fiducial sample of subhalos.

2.4 Quenching Models

As highlighted in §5.1, observations of low-mass galaxies in the local Universe suggest that all isolated (or "field") systems at $\lesssim 10^9$ $M_\odot$ are star-forming. Thus, all quenching at these low masses is likely driven by environmental effects associated with dwarf galaxies being accreted onto more massive halos, such as that of the Milky Way or M31. Two likely quenching mechanisms operating on satellite systems are starvation, where future gas accretion onto the satellite is halted following infall into a more massive host halo, and ram-pressure stripping, where the cold gas in a satellite galaxy is violently removed via interaction with the hot gas halo of the host. To mimic these respective processes, we implement two quenching models in the ELVIS simulations: (*i*) a "starvation" model in which quenching depends only on time since infall into the host halo and (*ii*) a "stripping" model in which quenching occurs once a satellite reaches a fixed physical distance from the host.

2.4.1 Starvation Model

When quenching occurs via starvation, the satellite galaxy is deprived of any additional supply of cold gas after infall, such that star formation is halted following the consumption of its current gas reservoir — i.e. quenching occurs within the gas depletion timescale ($\tau_{\rm depl} = M_{\rm gas}/{\rm SFR}$). While observations suggest that atomic and/or molecular depletion timescales may vary with galaxy mass [**? ? ? ?**], we adopt a fixed quenching timescale (following infall) over the limited stellar mass range probed in our analysis ($10^6 - 10^8$ $M_\odot$).

In the models, we define the infall time as the lookback time at which a halo *first* crosses

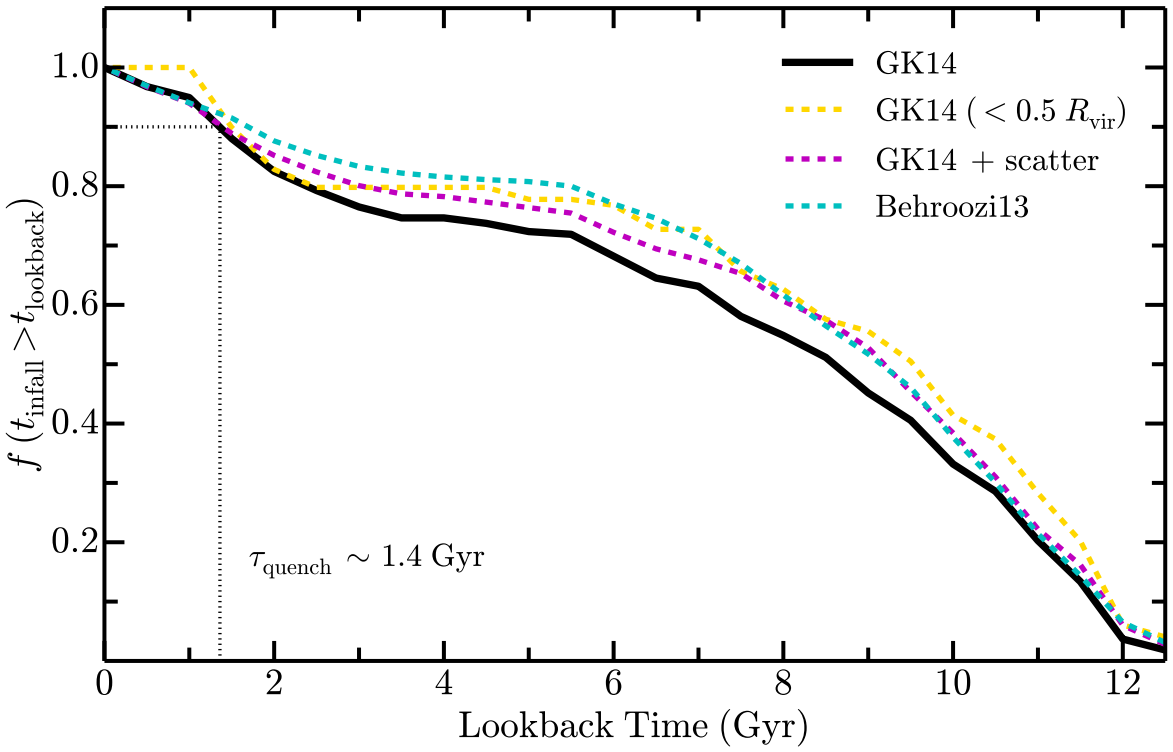

Figure 2.3: The cumulative distribution of infall times ($t_{\rm infall}$) as a function of lookback time for those subhalos in the ELVIS simulations identified as hosts of the Local Group satellites at $10^6 < {\rm M}_\star/{\rm M}_\odot < 10^8$. The solid black line corresponds to our default selection criteria, where subhalos are selected according to the abundance matching relation of **?**], restricting to those subhalos with $V_{\rm max}/V_{\rm peak} > 0.3$ and within the host virial radius at $z = 0$. The dashed cyan and magenta lines show the corresponding distribution of infall times when applying alternative abundance matching prescriptions (see §2.3), while the dashed gold line traces the accretion history of only those subhalos within 0.5 $R_{\rm vir}$ at $z = 0$ following the **?**] abundance matching relation. A quenched fraction of 90% today, as observed for the Local Group at these masses, corresponds to a quenching timescale ($\tau_{\rm quench}$) of ~ 1.4 Gyr.

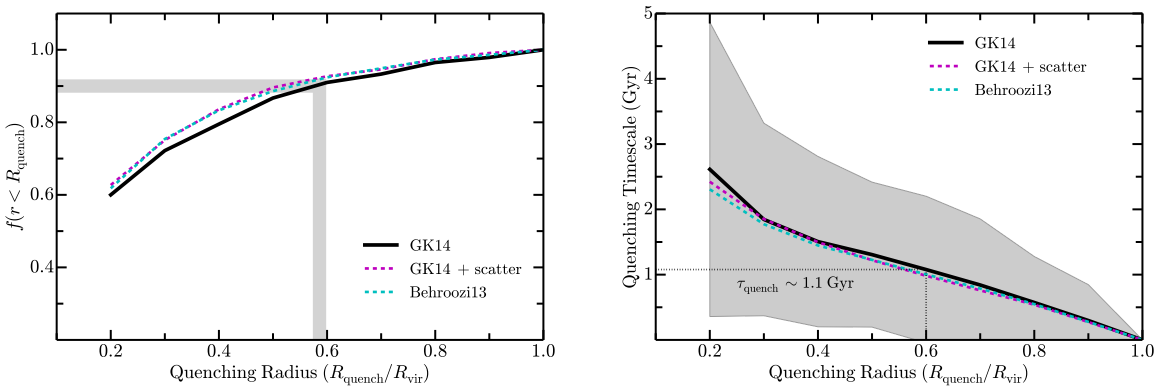

Figure 2.4: *Left*: The dependence of the satellite quenched fraction on the assumed quenching radius, $R_{\rm quench}$, for our ram-pressure stripping model (see §2.4.2). The solid black and dashed cyan and magenta lines correspond to subhalo populations selected according to different abundance matching prescriptions (see §2.3). In all cases, a quenching radius of 0.6 $R_{\rm vir}$ is required to reproduce a quenched fraction of 90% as observed in the Local Group. *Right*: The dependence of the mean quenching timescale ($\tau_{\rm quench}$) on the assumed quenching radius ($R_{\rm quench}$) for the same set of abundance matching relations. For our fiducial subhalo sample, the grey shaded region illustrates the 1σ scatter in the quenching timescale across the 48 ELVIS hosts. As for the starvation model, the high observed quenched fraction in the Local Group implies a short quenching timescale (~ 1.1 Gyr) in our ram-pressure stripping model. The typical $R_{\rm vir}$ (at $z = 0$) for ELVIS hosts is ~ 300 kpc.

the virial radius, $R_{\rm vir}(z)$, of the host. For the $\sim 23\%$ of subhalos that cross the host virial radius more than once, we are likely overestimating the infall time. However, 90% of these subhalos are accreted for a final time $\gtrsim 6$ Gyr ago, thereby contributing little to no effect on the final inferred quenching timescale. Figure 2.3 shows the cumulative distribution of infall times for subhalos selected as hosts of Local Group satellites in the simulations following various abundance matching prescriptions. Universally, we find that subhalos are accreted relatively uniformly over cosmic time, with the vast majority infalling into their host halo > 2 Gyr ago.

As shown in Figure 2.3, to match the observed satellite quenched fraction of $\sim 90\%$ in the Local Group, the starvation model – independent of the adopted abundance matching prescription – favors a quenching timescale ($\tau_{\rm quench}$) of roughly $1.4^{+0.9}_{-0.7}$ Gyr, including the error associated with the uncertainty in the observed Local Group quenched fraction (according to binomial statistics). Thus, on average, satellites of the Milky Way and M31 (at $M_\star \sim$

$10^6 - 10^8$ $M_\odot$) must quench within 1.4 Gyr of infalling onto their respective host halo. Within the individual ELVIS simulations there is non-negligible scatter in the derived quenching timescale, given the stochasticity of subhalo accretion events; assuming a quenched fraction of 90%, the 1σ scatter in $\tau_{\rm quench}$ across the 12 Local Group-like host pairs in ELVIS is approximately 0.7 Gyr.

A quenched fraction of 90% in the local group could be dependent on completeness of the dwarf sample in this mass range, as discussed in the introduction. This is particularly true around M31, where PAndAS imaging only surveys the volume within a radius of $\sim$ 150 kpc. To test the impact of this potential selection effect on our results, we also compute the distribution of infall times for those subhalos that reside within 0.5 $R_{\rm vir}$ today. While simulated subhalos with earlier infall times are slightly biased towards smaller host-centric distances [e.g. **? ? ?**], the correlation between radial distance from the host and infall time exhibits significant scatter, such that the quenching timescale derived from subhalos within 0.5 $R_{\rm vir}$ today is fully consistent with that based on the full sample of subhalos within 1 $R_{\rm vir}$ (see Fig. 2.3).

In our starvation model, it is assumed that the quenching timescale (i.e. depletion timescale) is independent of cosmic time. While studies at higher redshift are limited to significantly more massive systems, current work suggests that molecular depletion timescales are relatively weakly dependent on redshift [**? ? ? ?**], favoring shorter timescales at higher z. This conclusion is echoed in analysis of the satellite quenching timescale across a broad range of halo masses at intermediate redshift [**? ? ? ? ?**]. Altogether, a modest variation in the quenching timescale with redshift would yield no significant impact on our results, as our analysis is focused on the cumulative quenched fraction today and not on the detailed quenching times of individual satellites.

2.4.2 Stripping Model

To mimic quenching via ram-pressure stripping, we implement a model in which satellites are quenched at a fixed radial distance ($R_{\rm quench}$) from their host. In a stripping scenario, this radial quenching scale would be set by the volume over which the host's hot halo reaches a density capable of stripping an infalling dwarf. To account for growth of the hot halo over cosmic time, we define our quenching radius, $R_{\rm quench}$, in terms of the host's virial radius as a function of redshift (i.e. $R_{\rm quench} \propto R_{\rm vir}(z)$) and require that a subhalo cross within the quenching radius at $z < 3$, allowing the host's hot halo time to form [**?** **?** **?**]. For subhalos in ELVIS that have crossed within the quenching radius at $z < 3$, we classify the corresponding satellite as quenched; all other systems remain star-forming, independent of the time spent in the host halo (i.e. independent of infall time).

Figure 2.4a shows the dependence of the satellite quenched fraction on the adopted quenching radius (from 0.2 $R_{\rm vir}$ to 1 $R_{\rm vir}$). We find that to reproduce the observed quenched fraction in the Local Group (90%) requires a quenching radius of roughly 0.6 $R_{\rm vir}$, again with little dependence on the assumed abundance matching relation. Adopting this value for the quenching radius ($R_{\rm quench} = 0.6\ R_{\rm vir}$), we are able to determine the time at which each subhalo in the simulation (i.e. satellite) quenched following infall — and thus the quenching timescale (measured relative to infall). In Figure 2.4b, we show the mean quenching timescale as a function of the chosen quenching radius ($R_{\rm quench}$) within the 48 ELVIS simulations. For large values of $R_{\rm quench}$, each satellite – largely independent of orbit – spends little time in the host halo prior to being quenched, such that the effective quenching timescale ($\tau_{\rm quench}$) is short. Adopting a quenching radius of $R_{\rm quench} = 0.6\ R_{\rm vir}$, we find an average quenching timescale of 1.1 Gyr, in very good agreement with that derived from our starvation model (see §2.4.1). Finally, a complementary analysis by **?**], in which quenching commences at pericenter passage, finds very similar results [$\tau_{\rm quench} \sim 1 - 2$ Gyr, see also **?** **?**].

2.5 Discussion

Given that nearly all field dwarfs are star-forming at stellar masses of $\lesssim 10^9$ $M_\odot$ [**?** **?** **?**], environment-dependent processes are the dominant driver of quenching at low masses and must act on a timescale so as to avoid over- or under-producing the number of star-forming satellite galaxies in the Local Group. Independent of the particular physical mechanism(s) at play, the high quenched fraction ($\sim$ 90%) observed for low-mass Local Group satellites thereby dictates a remarkably short quenching timescale, measured relative to infall. Through a detailed comparison of the observed Milky Way and M31 satellites to the ELVIS suite of simulations, we show that this quenching timescale ($\tau_{\rm quench}$) is $\sim$ 2 Gyr at stellar masses of $10^6 - 10^8$ $M_\odot$ in the Local Group.

A very similar analysis by **?**], in which the properties of nearby dwarfs in the SDSS are compared to the Millennium-II simulation [**?**], finds that the quenching timescale must be much longer ($>$ 7.5 Gyr) at slightly higher stellar masses ($\sim 10^9$ $M_\odot$). This longer quenching timescale is dictated by the relatively low quenched fractions observed in nearby groups [**?**]. While **?**] preferentially study higher-mass host halos than that of the Milky Way and M31, analysis of the Local Group is in broad agreement. At $M_\star \sim 10^8 - 10^{10}$ $M_\odot$, the satellite quenched fraction in the Local Group is only $\sim$ 40% [**?** **?** **?**], which requires a quenching timescale of $\sim$ 7.8 Gyr when comparing the infall times of ELVIS subhalos selected to have $M_\star \sim 10^{8.5} - 10^{9.5}$ $M_\odot$ according to the abundance matching relation of [**?**].

In an effort to study quenching for the most massive satellite systems, **?**] and **?**] compare group and cluster populations from the SDSS [**?**] to N-body and semi-analytic models, respectively. While analysis at these masses is complicated by the fact that some isolated or field systems are quenched independent of any environment-related effects, these independent analyses conclude that the quenching timescale at $\sim 10^{10} - 10^{11}$ $M_\odot$ increases with decreasing satellite stellar mass, reaching as long as $\sim 5 - 6$ Gyr [see also **?**]. Interestingly, for these

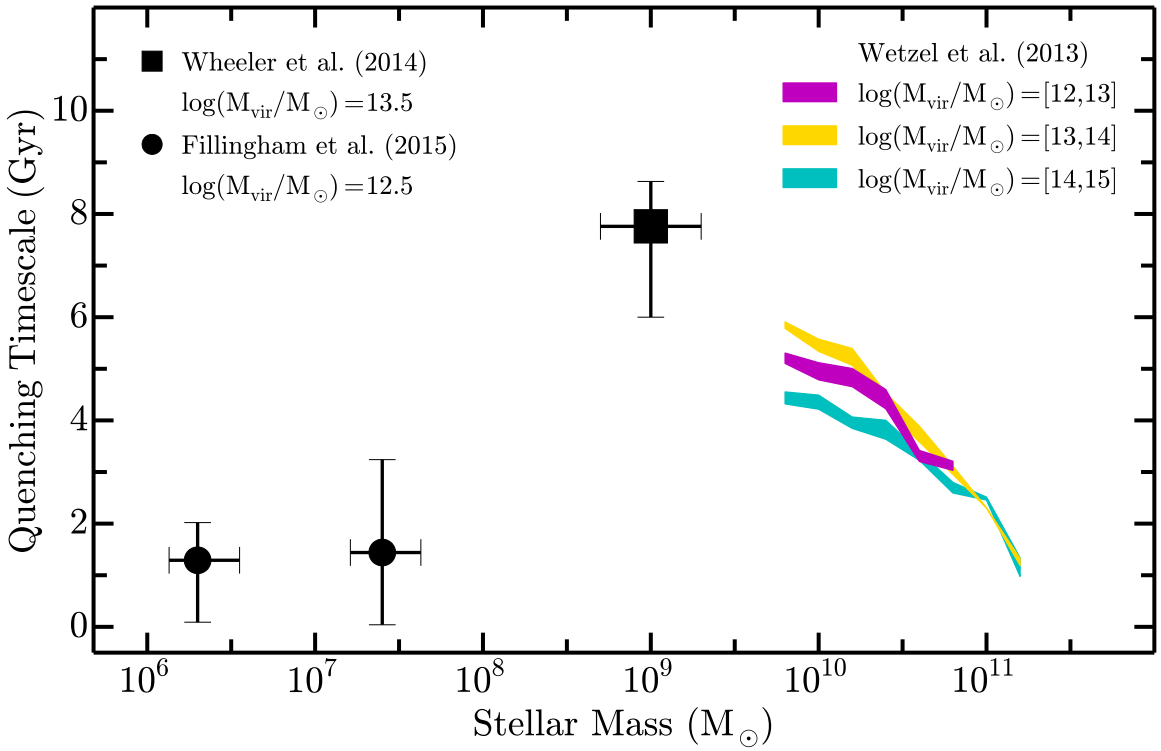

Figure 2.5: The dependence of the satellite quenching timescale ($\tau_{\rm quench}$) on satellite stellar mass at $M_\star \sim 10^6 - 10^{11}$ $M_\odot$. The inset legend lists the typical host halo mass for each data set. The magenta, gold, and cyan colored bands show the constraints for satellites in different mass host halos derived from analysis of galaxy groups and clusters in the SDSS by **?**]. The black square denotes the typical quenching timescale for slightly lower-mass satellites ($\sim 10^9$ $M_\odot$) from **?**], with the horizontal error bars denoting the $25-75\%$ range in stellar mass probed by that work and the vertical error bars giving the variation in $\tau_{\rm quench}$ corresponding to satellite quenched fractions of $25-55\%$ (as derived from analysis of subhalo populations in ELVIS, see §2.5). Our estimate for the low-mass satellite quenching timescale in the Local Group is given by the black circles ($\tau_{\rm quench} \sim 1.4$ Gyr, see §2.4.1), where our sample of subhalos is divided into two stellar mass bins of $10^6 - 10^7$ $M_\odot$ and $10^7 - 10^8$ $M_\odot$. Each point gives the quenching timescale for subhalos in that mass bin assuming a satellite quenched fraction of 90%, while the vertical error bars illustrate the variation in $\tau_{\rm quench}$ corresponding to satellite quenched fractions of $80-100\%$. Our results are largely independent of mass, with increased scatter at higher masses due to the smaller number (and thus increased stochasticity in the infall times) of massive subhalos. The horizontal error bars show the quartiles of the subhalo mass distribution within each bin. At high masses, the quenching timescale increases with decreasing stellar mass. Below $M_\star \sim 10^8$ $M_\odot$, we find that satellite quenching becomes dramatically more efficient, suggesting a likely change in the physical mechanisms at play.

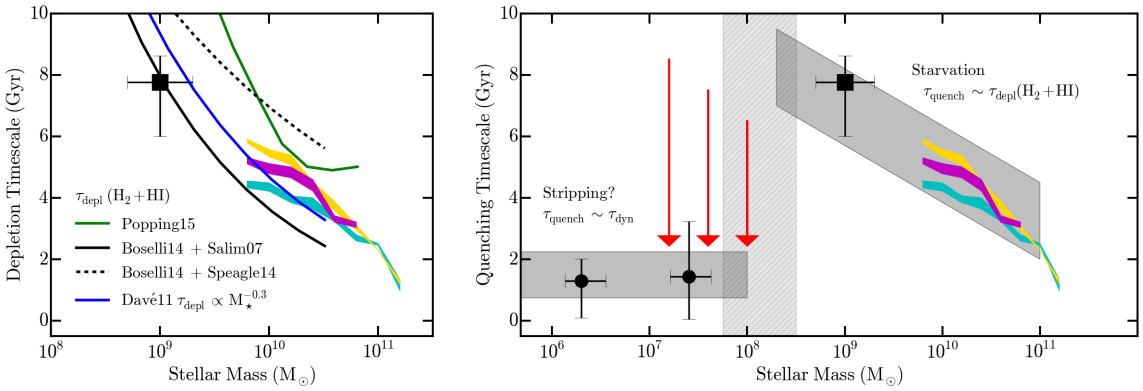

Figure 2.6: *Left*: The dependence of the satellite quenching timescale ($\tau_{\rm quench}$) and gas depletion timescale ($\tau_{\rm depl}$) on satellite stellar mass at $M_\star \gtrsim 10^8$ $M_\odot$. The magenta, gold, and cyan colored bands show the constraints for satellites in different mass host halos derived from analysis of galaxy groups and clusters in the SDSS by **?**]. The black square gives the typical quenching timescale for lower-mass satellites ($\sim 10^{8.5} - 10^{9.5}$ $M_\odot$) from **?**]. The solid and dashed black lines show the mass dependence of the gas depletion timescale (H_2 + HI) derived from combining the observed gas fractions of **?**] with the star formation rate-stellar mass relation of **?**] and **?**], respectively. The solid blue and solid green lines give the corresponding predictions from the hydrodynamical and semi-empirical models of **?**] and **?**], respectively. The inferred satellite quenching timescales at $\gtrsim 10^8$ $M_\odot$ show broad agreement with the observed gas depletion timescales for field systems, suggesting that starvation is the main driver of satellite quenching at these masses. *Right*: The dependence of the satellite quenching timescale on satellite stellar mass at $10^6 < M_\star/M_\odot < 10^{11}$, including the estimates of $\tau_{\rm quench}$ from Fig. 2.5. The light grey shaded regions highlight the expected dominant quenching mechanism and projected mass dependence of $\tau_{\rm quench}$, while the vertical hashed grey region demarcates the critical mass scale below which a more efficient physical process (e.g. ram-pressure stripping) drives relatively rapid quenching in the Local Group. At high masses ($\gtrsim 10^8$ $M_\odot$), satellite quenching is consistent with being driven by starvation; below $\sim 10^8$ $M_\odot$, however, we posit that ram-pressure stripping becomes increasingly effective, such that depletion (and thus quenching) timescales are significantly shorter.

most massive satellites, no evidence is found for variation in the quenching timescale with host halo mass [**?** , but see also **?**].

In Figure 2.5, we combine our estimate of the quenching timescale for low-mass satellites in the Local Group ($M_\star \sim 10^7$ $M_\odot$) with the complementary constraints from **?**] and **?**] at higher stellar masses. Due to differences in the adopted definiton of infall time (see discussion in **?**), we assume a quenching timescale of 8 Gyr at 10^9 $M_\odot$. This value for $\tau_{\rm quench}$ is fully consistent with the results from **?** , $\tau_{\rm quench} \sim 7.5 - 9$ Gyr]; as previously highlighted,

analysis of higher-mass subhalos in the ELVIS simulations — systems corresponding to $10^{8.5} - 10^{9.5}$ $M_\odot$ following the **?**] abundance matching relation — yields a very similar result ($\tau_{\rm quench} \sim 7.8$ Gyr; see also **?**). Altogether, we find that the quenching timescale increases with decreasing mass at $\gtrsim 10^8$ $M_\odot$, such that environmental processes are relatively inefficient in suppressing star formation at $\sim 10^9$ $M_\odot$. At lower stellar masses ($\lesssim 10^8$ $M_\odot$), however, the quenching timescale decreases dramatically, indicating a stark increase in the satellite quenching efficiency for low-mass systems. Given that all known satellites of the Milky Way and M31 are quenched below stellar masses of $\sim$ a few $\times$ 10^5 $M_\odot$, the quenching timescale is expected to remain short to even lower masses. For the lowest-mass systems (i.e. ultra-faint dwarfs) environmental quenching is likely irrelevant, as the smallest dark matter halos may have their star formation suppressed significantly by non-environmental mechanisms like cosmic reionization [e.g. **?** **?** **?** **?**].

For an infalling satellite of any mass, assumed to be isolated from subsequent gas accretion, an upper limit on the longevity of any star formation activity is set by the gas supply within the satellite upon infall — including the satellite's hot halo, from which gas may cool. Processes such as ram-pressure stripping, tidal effects, and harassment would then work to diminish this gas supply, so as to accelerate the quenching process. The long quenching timescales observed for higher-mass satellites ($\sim 10^8 - 10^{10}$ $M_\odot$) thus favor starvation as the dominant quenching mechanism. Ignoring future accretion, recycling, or gas cooling, the duration of star formation should follow the gas depletion timescale ($\tau_{\rm depl} = M_{\rm gas}/{\rm SFR}$, where $M_{\rm gas}$ is the mass of a satellite's cold gas reservoir upon infall). While studies of nearby star-forming galaxies suggest that the surface density of ongoing star formation is most closely tied to the dense H_2 gas [**?** **?** **?**], observed molecular depletion timescales are much shorter than the inferred quenching timescales. For relatively massive galaxies ($M_\star \gtrsim 10^{10}$ $M_\odot$), spanning a broad range of redshift, current observations point towards molecular depletion timescales of roughly $1 - 2$ Gyr [**?** **?** **?** **?** **?** **?** **?**]. Moreover, recent work targeting larger samples of lower-mass galaxies conclude that the molecular depletion

timescale decreases with decreasing stellar mass, such that infalling satellites at 10^9 $M_\odot$ should, on average, exhaust their molecular reservoirs in less than 1 Gyr [**?** **?**].

These relatively short molecular depletion timescales are in direct conflict with the derived quenching timescales for satellites at $\sim 10^9 - 10^{10}$ $M_\odot$, which indicate that star formation typically continues for > 4 Gyr after infall. Given that strong variation in star-formation efficiency for H_2 is disfavored by both observations of the Kennicutt-Schmidt relation [**?** **?** **?**] and the bimodality of rest-frame galaxy colors [or specific star formation rates, **?** **?**],[2] the extended star formation in satellite galaxies seemingly must be driven by a fuel supply beyond the molecular reservoir. While gas cooling from a satellite's hot halo could replenish the fuel supply for star formation, there is little observational evidence for significant hot gas coronae around star-forming galaxies, even at the high-mass regime and especially when restricting to gas with a sufficiently short cooling time [**?** **?** **?** **?**].

On the other hand, if atomic gas is included as a potential fuel source for star formation, there may be better agreement between the expected gas depletion and satellite quenching timescales. As previously stated, star formation is observed to follow molecular gas density more closely than atomic gas density, although the weaker correlation with HI surface density could be largely due to atomic gas spanning a broader range of densities, thus on average tracing dense star-forming clouds more poorly [**?** **?** **?**]. As shown in Figure 2.6a, when including the atomic gas component, the inferred quenching timescales at high stellar masses ($M_\star \gtrsim 10^8$ $M_\odot$) are in broad agreement with the measured and predicted (atomic plus molecular) gas depletion timescales and thus consistent with a picture where satellite quenching is driven by starvation at high masses.

In the low-mass regime ($\lesssim 10^8$ $M_\odot$), the atomic component becomes increasingly important, with observations of nearby star-forming systems finding that the typical HI gas fraction

[2]While a reduction in the star formation efficiency for satellites would yield longer depletion (and thus quenching) timescales, it would also lead to overproducing galaxies in the "green valley".

increases steadily towards lower mass [**?** **?** **?** **?** **?** **?**]. More importantly, this relative growth in atomic gas outpaces the corresponding increase in the average specific star formation rate [e.g. **?** **?** **?**], such that the gas depletion timescale is generally long ($\gtrsim$ 10 Gyr) for low-mass star-forming galaxies — a result that is fully consistent with the dearth of quiescent field galaxies at $< 10^9$ $M_\odot$ [**?** **?**]. In comparison to the typical quenching timescales at low masses, however, the overabundance of atomic gas in these systems suggests that starvation alone cannot drive satellite quenching at $\lesssim 10^8$ $M_\odot$. Instead, a secondary process, such as ram-pressure stripping, is needed to remove cool gas from infalling systems, thereby decreasing the gas depletion timescale significantly.

As observations of systems such as Leo I suggest [**?**], we would expect stripping to occur as a satellite infalls from $R_{\rm vir}$ towards pericenter, such that quenching at low masses would proceed according to the dynamical time ($\tau_{\rm dyn}$), which is roughly $1 - 2$ Gyr for a Milky Way-like halo today [e.g. **?**]. While a detailed analysis of the efficacy of ram-pressure stripping (or other quenching mechanisms such as tidal forces) is beyond the scope of this work (see Fillingham et al. in prep), Figure 2.6b presents a qualitative depiction of the potential physical processes at play, where satellite quenching is primarily driven by starvation at higher masses ($\gtrsim 10^8$ $M_\odot$ for the Local Group) while ram-pressure stripping becomes increasingly effective below a critical mass scale of $\sim 10^8$ $M_\odot$, yielding shorter quenching timescales and high observed quenched fractions. In this qualitative picture, we expect that ram-pressure stripping (or some other efficient quenching mechanism) plays a critical role in suppressing star formation down to the mass scales at which reionization inhibits gas accretion and therefore star formation [perhaps, $M_\star \sim 10^4$ $M_\odot$, **?** **?** **?**]. Applying this qualitative picture to higher-mass host halos (e.g. rich groups and clusters), the critical scale at which ram-pressure stripping becomes effective should move to higher satellite masses due to the increased density of the host's hot halo in concert with higher infall velocities for the satellites.

2.6 Summary

Comparing observations of the Local Group satellite population to corresponding high-resolution N-body simulations from the ELVIS suite, we investigate the typical timescale (following infall) upon which star formation is suppressed in low-mass ($< 10^8$ $M_\odot$) satellite galaxies. When combining our work with complementary analyses of higher-mass satellite populations, we present a comprehensive picture of satellite quenching spanning roughly five orders of magnitude in stellar mass. Our principal results are as follows:

- To reproduce the high fraction of quenched low-mass satellites in the Local Group, the typical quenching timescale at $M_\star \sim 10^6 - 10^8$ $M_\odot$ must be relatively short ($\tau_{\rm quench} \sim 2$ Gyr).

- The longer quenching timescales inferred for higher-mass satellites are roughly consistent with the observed cold gas (H_2 plus HI) depletion timescales in corresponding field systems; this suggests that satellite quenching is largely driven by starvation at $M_\star \gtrsim 10^8$ $M_\odot$.

- At low masses ($M_\star \lesssim 10^8$ $M_\odot$), the much shorter satellite quenching timescales are potentially set by ram-pressure stripping or some other process that removes the cold gas reservoirs in infalling systems, such that nearly all low-mass satellites in the Local Group (or more massive host halos) are quenched.

- If ram-pressure stripping is responsible for increasing the satellite quenching efficiency at low masses ($M_\star \lesssim 10^8$ $M_\odot$) within the Local Group, we expect that this critical quenching scale will shift to higher satellite masses in higher-mass host halos (e.g. rich groups and clusters) due to the increased density of the host's hot halo in concert with higher infall velocities for the satellites.

We have suggested here that the transition to rapid quenching in the smallest satellites

($M_\star \lesssim 10^8\ M_\odot$) is potentially explained as a ram-pressure scale (see Figure 2.6 and Fillingham et al. in prep). Above this scale, satellite quenching occurs on a gas depletion time, as accreted galaxies are starved of fresh fuel for star formation. Below this scale, a more rapid, drag-induced stripping becomes dominant, such that the gravitational restoring force of lower-mass dark matter halos can no longer retain cool gas against the fluid pressure they experience while in orbit around a larger host.

The idea that Local Group dwarfs are quenched via ram pressure has been around for some time [e.g. **? ? ?**] but the evidence for very rapid quenching provided here adds further argument in its favor, and identifies a characteristic mass scale where it may become dominant. Underlying this hypothesis is the notion that the Milky Way and M31 both harbor extended (~ 150 kpc) reservoirs of hot baryons with sufficient density to strip small galaxies of their gas. There is evidence that M31 does indeed host an extended circumgalactic medium [**?**], and X-ray studies are consistent with this possibility around the Milky Way [**? ? ?**]. If extended low-density coronae of this kind are common around $\sim L^*$ galaxies, then they may prove important for understanding the baryon cycle and the global census of baryons in the Universe.

Of course, one shortcoming of our analysis is that we have restricted ourselves to satellites of M31 and the Milky Way. Given completeness issues, the Local Group is a reasonable starting point, but it remains possible that satellites in our vicinity are unusually quenched, perhaps owing to an uncommonly dense distribution of hot baryons in our vicinity, or atypically early infall times for the Local Group satellite population. Ongoing efforts to discover and characterize dwarf satellite systems around other massive hosts will be important for solidifying the existence of a sharp transition scale at $M_\star \lesssim 10^8\ M_\odot$, where satellite quenching appears to become extremely efficient in the Local Group. If future studies reveal that the Local Group is indeed typical, then pinpointing the origin of this quenching scale and testing the ram-pressure hypothesis will be of utmost importance.

Chapter 3

Under Pressure: Quenching Star Formation in Low-Mass Satellite Galaxies via Stripping

3.1 Introduction

Recent studies probing the properties of satellite galaxies in the local Universe show that the suppression (or "quenching") of star formation in satellites is a relatively inefficient process relative to the expectations of hydrodynamic and semi-analytic models of galaxy formation [e.g. **? ? ? ? ?**]. While satellites are rapidly quenched – following infall – in the models, analysis of satellite populations identified in the Sloan Digital Sky Survey [SDSS, **?**] instead find that quenching proceeds remarkably slowly, such that a typical satellite with $M_\star \gtrsim 10^8$ $M_\odot$ orbits within its host halo – continuing to form stars – for $\sim 3-7$ Gyr before being quenched [**? ? ?**].[1] Only at the lowest satellite masses is quenching a highly

[1]These measured satellite quenching timescales include the transition of a satellite system from star-forming to quiescent, which must proceed quickly (within ~ 1 Gyr) so as to reproduce the observed bimodal

efficient process, with low-mass ($M_\star < 10^8$ $M_\odot$) satellites in the Local Group quenching within $\sim 1-2$ Gyr of infall [**?** **?** **?**].

In an effort to connect these measured quenching timescales to the relevant physical mechanisms at play, **?**] present a comprehensive picture of satellite quenching spanning roughly 5 orders of magnitude in satellite stellar mass. The low efficiency and long quenching timescales inferred for intermediate- and high-mass satellites ($M_\star \gtrsim 10^8$ $M_\odot$) are consistent with quenching via starvation – a scenario in which gas accretion on to a satellite galaxy is halted following infall, thus eventually eliminating the fuel for star formation [**?** **?**]; lending support to this picture, the measured quenching timescales agree very well with the observed cold gas (HI + H_2) depletion timescales for field systems at $z \sim 0$ [**?**]. At lower satellite masses ($M_\star \lesssim 10^8$ $M_\odot$), however, the quenching timescales derived from analysis of the Local Group satellite population suggest that the physics of satellite quenching must change significantly; a more efficient quenching mechanism (relative to starvation) must be at play below a critical mass scale of $\sim 10^8$ $M_\odot$.

Stripping is a plausible candidate quenching mechanism at low masses. This includes ram-pressure stripping [**?**], a process by which the cool, dense interstellar medium (and thus the fuel for future star formation) is removed from a satellite galaxy as it passes through its host's circumgalactic medium (CGM). Ram-pressure stripping becomes increasingly effective in lower-mass satellites, due to their weaker gravitational restoring pressures [**?**]; moreover, ram pressure acts on roughly the dynamical time of the host system [i.e. $1-3$ Gyr, **?** **?**], consistent with the short quenching timescale inferred for low-mass satellites of the Local Group. In addition to ram-pressure stripping, cold gas may also be removed from a satellite due to turbulent viscous stripping, which results from Kelvin-Helmholtz instabilities at the interface of the satellite's interstellar medium and the CGM [**?**]. The relative motion of the two media in addition to the substantial difference in their mean densities can lead to

distribution of specific star-formation rates and rest-frame colors [**?** **?**].

perturbations that overcome the local gravitational restoring force, such that gas is stripped from the satellite. Within massive groups and clusters, a wide range of observations provide abundant evidence of stripping in action, showing its ability to quench infalling galaxies via removal of their cold gas component [e.g. **? ?**]. It remains uncertain, however, if stripping is an effective quenching mechanism in more typical host halos, such as that of the Milky Way or M31, and specifically at satellite stellar masses of $\lesssim 10^8$ $M_\odot$.

In this work, our goal is to directly address the efficacy of stripping as a quenching mechanism for low-mass satellites in Milky Way-like systems. By using observations of local field dwarfs to inform analytic calculations of both ram-pressure and turbulent viscous stripping, we measure the amount of cold gas that would typically be removed *if* these field dwarfs were to interact with a Milky Way-like host. In Section 3.2, we detail our methods, including the analytic framework and data sets that we utilize to estimate the impact of stripping on infalling satellites. In Section 4.3, we present our primary results regarding the efficiency of stripping in Milky Way-like environments, specifically addressing potential uncertainties associated with the properties of the host halo and the satellite population. Finally, in Sections 4.4 and 4.5, we discuss and summarize the implications of our results with regard to the quenching of low-mass satellites in the Local Group and beyond.

3.2 Testing Satellite Stripping

3.2.1 Analytic Framework

The effectiveness of stripping as a quenching mechanism boils down to a relatively simple competition between the stripping pressure ($P_{\rm stripping}$) and the gravitational restoring force per unit area (i.e. the gravitational restoring pressure, $P_{\rm restore}$). When $P_{\rm restore} \geq P_{\rm stripping}$, the interstellar medium (or ISM, comprised predominantly of cold gas) is retained by the infalling

satellite galaxy, such that star formation may proceed. When the stripping pressure exceeds the gravitational restoring pressure, however, some fraction of the cold gas is removed from the satellite. In cases where this stripped fraction is large enough, star formation will be shut down rapidly due to the loss of available fuel. In what follows, we investigate two different mechanisms for removing the cold interstellar medium of infalling satellites.

Ram-Pressure Stripping

Following **?**], we estimate the ram pressure ($P_{\rm ram}$) as:

$$P_{\rm ram} \sim \rho_{\rm halo} V_{\rm sat}^2 \ , \tag{3.1}$$

where $\rho_{\rm halo}$ is the density of the host's gas halo and $V_{\rm sat}$ is the velocity of the satellite galaxy with respect to the host's frame of reference, or more precisely the local reference frame of the host's gas halo in the immediate vicinity of the infalling satellite galaxy. As shown in Equation 3.1, the ram pressure experienced by an infalling satellite is dependent on the local environment — thus, the properties of the host system, in particular its dark matter halo mass, which plays a critical role in setting $\rho_{\rm halo}$ and $V_{\rm sat}$. As described in Section 3.2.2, we utilize N-body simulations and observations of the Local Group and similar systems to inform our selection of these global environmental parameters, applying average values of $\rho_{\rm halo}$ and $V_{\rm sat}$ to all infalling satellites in our analysis. The adopted values for these parameters, along with uncertainties or biases that their selection introduces, are discussed directly in Section 3.3.2.

Assuming a spherical mass profile for an infalling satellite, the gravitational restoring force per unit area is given by:

$$P_{\rm restore} \sim \Sigma_{\rm gas}(r) \frac{G\,M(r)}{r^2} \ , \tag{3.2}$$

where $\Sigma_{\rm gas}(r)$ is the surface density of the cold gas to be stripped from the satellite and $M(r)$ is the total satellite mass interior to the radius r. As shown in Equation 3.2, the restoring pressure depends exclusively on the properties of the infalling galaxy, varying from one satellite system to the next, as it is accreted onto the parent halo. To model the properties of a representative sample of infalling satellites, we utilize observational data for a broad collection of nearby galaxies, including mass modeling to infer the local gravitational potential on a system-by-system basis (see Section 3.2.3).

For an infalling satellite, the degree to which ram pressure is able to strip its ISM is determined by the relative magnitude of the two pressures ($P_{\rm ram}$ versus $P_{\rm restore}$), such that stripping will occur beyond a radius r (within the satellite) if

$$\rho_{\rm halo} V_{\rm sat}^2 \ > \ \Sigma_{\rm gas}(r) \frac{G\,M(r)}{r^2} \ . \tag{3.3}$$

Throughout this work, we define $R_{\rm strip}$ as the innermost radial distance at which this inequality holds. Inside $R_{\rm strip}$, the restoring pressure is able to resist stripping, while ram pressure dominates beyond this radius.

Turbulent Viscous Stripping

The interaction at the interface of the ISM and the CGM can result in the growth of Kelvin-Helmholtz (K-H) instabilities due to the relative motion between the two phases. This will allow turbulent viscous stripping to remove the outer regions of the ISM when the gravitational restoring force is sufficiently small. Perturbations with wavenumber, k, are unstable if they meet the following criteria [**?** **?**]:

$$k > g \, \frac{\rho_{\rm gas}^2 - \rho_{\rm halo}^2}{\rho_{\rm gas}\, \rho_{\rm halo}\, V_{\rm sat}^2} \ , \tag{3.4}$$

where g is the gravitational restoring force at the ISM-CGM interface.

Previous studies of turbulent viscous stripping find that the dominant wavelength is set by the size of the cold gas region ($R_{\rm ISM}$), such that $k = 2\pi/R_{\rm ISM}$ [**?** **?**]. In our analysis, we make the assumption that $\rho_{\rm halo} \ll \rho_{\rm gas}$, which is undoubtedly true for gas-rich dwarfs accreted into the Local Group (or similar environments). Plugging these approximations into Equation 3.4, leads to the following inequality of the same form as Equation 3.3:

$$\rho_{\rm halo} V_{\rm sat}^2 \ > \frac{G\, M_0\, \bar{\rho}_{\rm gas}}{2\pi\, R_{\rm ISM}} \ , \tag{3.5}$$

where $\bar{\rho}_{\rm gas}$ is the average ISM density inside $R_{\rm ISM}$, and M_0 is the total restoring mass inside $R_{\rm ISM}$. If this inequality is true, then turbulent viscous stripping will proceed and the outer layers of the ISM will be removed. When this inequality is false, the gravitational restoring pressure is able to stabilize the outer layers of the ISM against the K-H instabilities.

When turbulent viscous stripping is able to proceed, the rate at which the ISM is removed will determine how much gas is stripped and ultimately whether the reservoir for star formation will be significantly depleted. The rate of total gas mass loss ($\dot{M}$) is given in slightly different forms throughout the literature [e.g. **?** **?** **?**]. In this work, we adopt the following approximation from **?**]:

$$\dot{M} \approx 20 \left(\frac{R_{\rm ISM}}{20\,{\rm kpc}}\right)^2 \left(\frac{n_{\rm halo}}{10^{-3}\,{\rm cm}^{-3}}\right) \left(\frac{V_{\rm sat}}{1000\,{\rm km\,s}^{-1}}\right) \frac{{\rm M}_\odot}{\rm yr} \ . \tag{3.6}$$

The details regarding how Equations 3.5 and 3.6 are used to determine the fraction of ISM removed from an infalling dwarf galaxy are discussed further in Section 3.2.4.

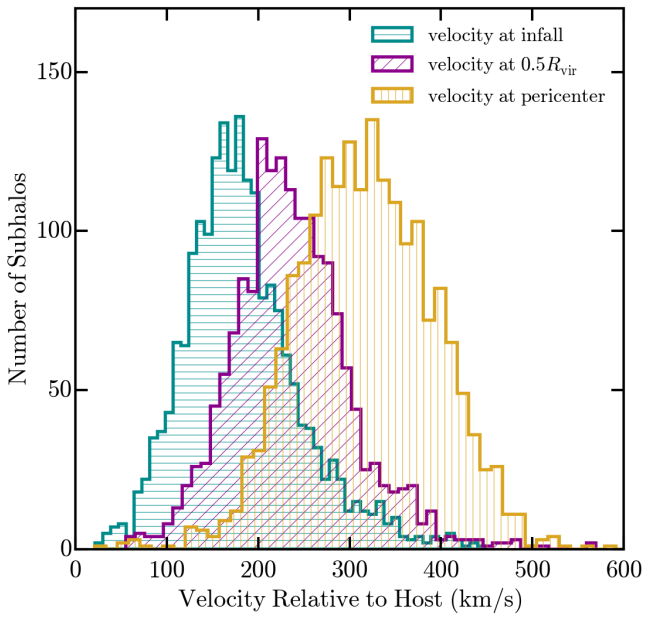

Figure 3.1: The distribution of subhalo velocities (relative to their parent halo) in the ELVIS suite of Local Group simulations for all subhalos that reside inside the virial radius at $z = 0$. The cyan, magenta, and gold histograms correspond to subhalo velocities measured when crossing the virial radius (i.e. infall), at 0.5 $R_{\rm vir}$, and at pericenter, respectively. For Milky Way-like systems, the typical satellite velocity (relative to the host's halo gas) is roughly $200 - 400$ km s^{-1} at the time of quenching. In our analysis, we adopt a fiducial value of $V_{\rm sat} = 300$ km s^{-1}.

3.2.2 Estimating $\rho_{\rm halo}$ and $V_{\rm sat}$

The strength of the stripping force acting upon an infalling satellite is primarily set by the density of the host's halo gas along with the relative velocity of the satellite (see Eq. 3.1 and Eq. 3.5). Within the Milky Way, a variety of indirect probes point towards halo gas densities of $\sim 10^{-4}$ cm^{-3} for the hot ($T \sim 10^6$ K) component [e.g. **? ? ? ? ?**]. Moreover, both observed X-ray emission and pulsar dispersion measurements in the Milky Way are consistent with a cored hot halo distribution with a density of $> 10^{-4}$ cm^{-3} extending to radial distances of ~ 100 kpc [**?** , see also **? ? ? ? ?**].

While the Milky Way's hot halo component is clearly important with regard to stripping in the Local Group, it is the density of the host's halo gas – across all temperatures – that dictates the strength of the stripping force. When folding in cooler phases of the circumgalactic medium, recent studies of nearby massive galaxies, comparable to the Milky Way, find halo gas densities of $\sim 10^{-3.5}$ cm^{-3} extending to at least $\gtrsim 0.25\ R_{\rm vir}$ [**? ? ?**]. These results are also supported by the latest analysis of the CGM surrounding M31 using quasar absorption-line spectroscopy, which finds evidence for a massive and extended gas halo [**?**]. Related studies targeting more massive, high-z systems find extended, high-density reservoirs of cool (10^4 K) halo gas reaching out to large fractions of the virial radius [**?**]. In accordance with these recent results, we assume a fiducial value for the host halo density ($n_{\rm halo}$) of $10^{-3.5}$ cm^{-3}, where $\rho_{\rm halo} = \mu n_{\rm halo} m_{\rm H\,I}$. For the purposes of this analysis, the mean molecular weight, μ, is set to 1.

Given the significant uncertainties in the observed halo densities of the Milky Way and M31, we explore how both our calculations of instantaneous ram-pressure stripping and continuous viscous stripping depend on this adopted value of $n_{\rm halo}$ in Section 3.3.2. Throughout our analysis, we make no assumptions regarding the radial profile of the halo gas. Given the expected orbits of infalling satellite populations and the existing constraints on the quenching

timescale measured relative to infall, however, there are relevant constraints regarding the extent of the CGM, which we discuss in Section 3.4.4.

To estimate the relative velocity of a satellite system in relation to the host's halo gas ($V_{\rm sat}$), we study the distribution of subhalo velocities within the Exploring the Local Volume In Simulations (ELVIS) suite of 48 high-resolution, dissipationless simulations of Milky Way-like halos [**?**]. The ELVIS suite includes 24 isolated halos as well as 12 mass-matched Local Group-like pairs, simulated within high-resolution uncontaminated volumes spanning $2-5$ Mpc in size using a particle mass of 1.9×10^5 M$_\odot$ and a Plummer-equivalent force softening of $\epsilon = 141$ physical parsecs. Within the high-resolution volumes, the halo catalogs are complete down to $M_{\rm halo} > 2\times10^7$ M$_\odot$, $V_{\rm max} > 8$ km s^{-1}, $M_{\rm peak} > 6\times10^7$ M$_\odot$, and $V_{\rm peak} > 12$ km s^{-1} – thus more than sufficient to track the evolution of halos hosting the Local Group dwarf population.

From ELVIS, we select subhalos corresponding to satellites with stellar masses of 10^6-10^9 M$_\odot$ — i.e. halo masses of $10^{9.7}-10^{11.2}$ M$_\odot$ following the stellar mass-halo mass (SMHM) relation of **?**]. We sample the velocities of these subhalos at the time of infall (i.e. crossing $R_{\rm vir}$), at 0.5 $R_{\rm vir}$, and at pericenter. In Figure 3.1, we show the distribution of subhalo velocities (relative to that of their host dark matter halo) at each of these distances. As expected, the average velocity of the subhalo population increases from infall towards pericenter, with a mean velocity of 183, 237, and 318 km s^{-1} at $R_{\rm vir}$, 0.5 $R_{\rm vir}$, and $R_{\rm peri}$, respectively.[2] To increase the precision at which we are able to measure the position of pericentric passage and the velocity at pericenter for each subhalo, we 3-d spline interpolate the position and velocity information for all subhalos across the 75 simulation snapshots in ELVIS. While this interpolation scheme achieves a time resolution of ~ 20 Myr, our resulting measurements of $R_{\rm peri}$ and $V_{\rm peri}$ are likely somewhat over- and under-estimated, respectively.

[2]Both the subhalo velocity and pericenter distributions show no dependence on subhalo mass, consistent with the idea that the host potential is the primary driver of these subhalo properties.

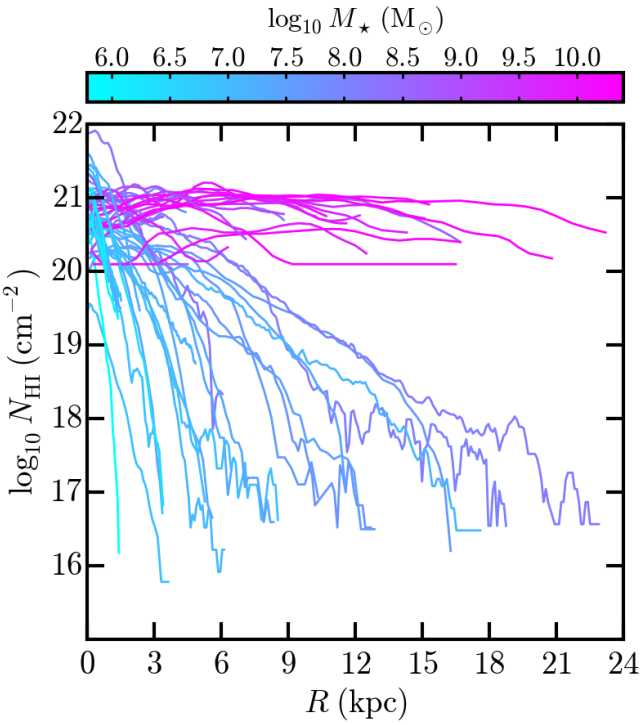

Figure 3.2: The observed HI surface density profiles for our sample of 66 nearby field galaxies from THINGS, Little THINGS, and SHIELD, color-coded according to the stellar mass of each system. While there is substantial scatter in profile shape from object to object, the lower-mass dwarfs are preferentially less extended than their more massive counterparts.

Typically, studies of instantaneous ram-pressure stripping assume the satellite velocity at pericenter, where stripping is expected to be greatest. Quenching (i.e. stripping) when a satellite reaches a radial distance of $\sim 0.5\ R_{\rm vir}$ while on first infall, however, is consistent with the inferred quenching timescales for the Local Group satellite population [**?**]. Herein, we compromise between these two scenarios, adopting a fiducial satellite velocity ($V_{\rm sat}$) of 300 km s^{-1}. In Section 3.3.2, we explore how our results depend upon this choice of $V_{\rm sat}$.

3.2.3 Estimating $\Sigma_{\rm gas}(r)$ and $M(r)$

As shown in Equation 3.2, the gravitational restoring pressure is dependent upon the properties of the infalling satellite, specifically the gas surface density and total mass profiles. To estimate these parameters for a representative sample of infalling satellites, we utilize existing

observations of 66 nearby, star-forming dwarf galaxies from the THINGS, Little THINGS, and SHIELD data sets (**?** **?** **?** ; McNichols et al. in prep; Teich et al. in prep). This sample is dominated by isolated (or "field") systems, for which the ISM is largely unaltered by previous interactions with a more massive host system — i.e. ideal candidates to test the effectiveness of ram-pressure stripping as a quenching mechanism. While the satellites of the Milky Way and M31 were primarily accreted at $z \sim 0.5 - 1$ [**?** **?**], our sample of nearby galaxies is expected to be similar in cold gas (specifically HI) content to similar systems at intermediate redshift [**?** **?**].

For galaxies drawn from Little THINGS and SHIELD, we infer the stellar mass of the system using the published V-band absolute magnitudes [**?** **?**] and assuming a mass-to-light ratio of unity, which is roughly consistent with the expectations for a ~ 1 Gyr-old simple stellar population following a Salpeter initial mass function [e.g. **?**]. For those systems selected from THINGS, we utilize the stellar mass estimates of **?**], which are derived from *Spitzer* 3.6μm imaging assuming a K-band mass-to-light ratio of 0.5. As discussed further in Section 3.3.1, uncertainties in the measured stellar masses for our sample have little impact on the quantitative or qualitative results of our analysis. For the 12 galaxies in the SHIELD sample, the resulting stellar mass estimates are in relatively good agreement with those derived from stellar population fits to multi-band *Hubble Space Telescope* photometry, with a typical offset (to higher masses) of 0.37 dex [**?**]. Altogether, the sample of 66 field systems spans a broad range in stellar mass, from $\sim 10^6 - 10^{11}$ $M_\odot$, covering the mass regime where **?**] find evidence for a change in the dominant satellite quenching mechanism and where stripping is presumed to become effective.

For each of the galaxies in our sample, we utilize the published HI surface density profiles from the THINGS, Little THINGS, and SHIELD projects, scaled by a factor of 1.36 to account for helium (**?** **?** **?** ; Teich et al. in prep). For a typical low-mass galaxy, the cold gas component is largely dominated by atomic (versus molecular) gas [e.g. **?** **?**], such that $\Sigma_{\rm HI}$ provides

a robust estimate of the ISM surface density and thus the efficacy of both ram-pressure and turbulent viscous stripping. As shown in Figure 3.2, the $\Sigma_{\rm HI}$ profiles for our sample exhibit significant variation in shape, with more massive systems having preferentially more extended HI surface density profiles. While the depth of the HI observations varies from object to object in our sample, the THINGS, Little THINGS, and SHIELD measurements are sensitive to the bulk of the atomic gas component, such that any undetected low-density gas at large radii would have a negligible impact on our stripping calculations.

To determine the mass profile, $M(r)$, for each galaxy in our sample, we infer the total dark matter halo mass according to the stellar mass-halo mass relation of **?**] and assume an NFW density profile [**?**] with a concentration given by the $c-M$ relation of **?**]. While this methodology neglects contributions to the mass profile from the baryonic component, these are relatively modest at these mass scales (i.e. $M_\star < 10^{11}$ $M_\odot$), as illustrated in Section 3.3.1. Recognizing current uncertainties in the dark matter density profiles of low-mass galaxies [e.g. **?** **?** **?** **?**], we also employ mass profiles derived from dynamical modeling of the observed HI kinematics for a subset of our systems, including NFW fits to the THINGS and Little THINGS samples from **?**] and **?**] as well as fits to a Burkert profile [**?**] from **?**].

3.2.4 Measuring the Stripped Fraction ($f_{\rm stripped}$)

Using the HI surface density profiles presented in Figure 3.2, we determine the fraction of HI gas stripped from each satellite in our sample, given an assumed host halo density ($\rho_{\rm halo}$), satellite velocity ($V_{\rm sat}$), and satellite mass profile ($M(r)$). Throughout our analysis, we first determine the amount of ISM removed via instantaneous ram-pressure stripping, then we allow turbulent viscous stripping to proceed for up to 1 Gyr.

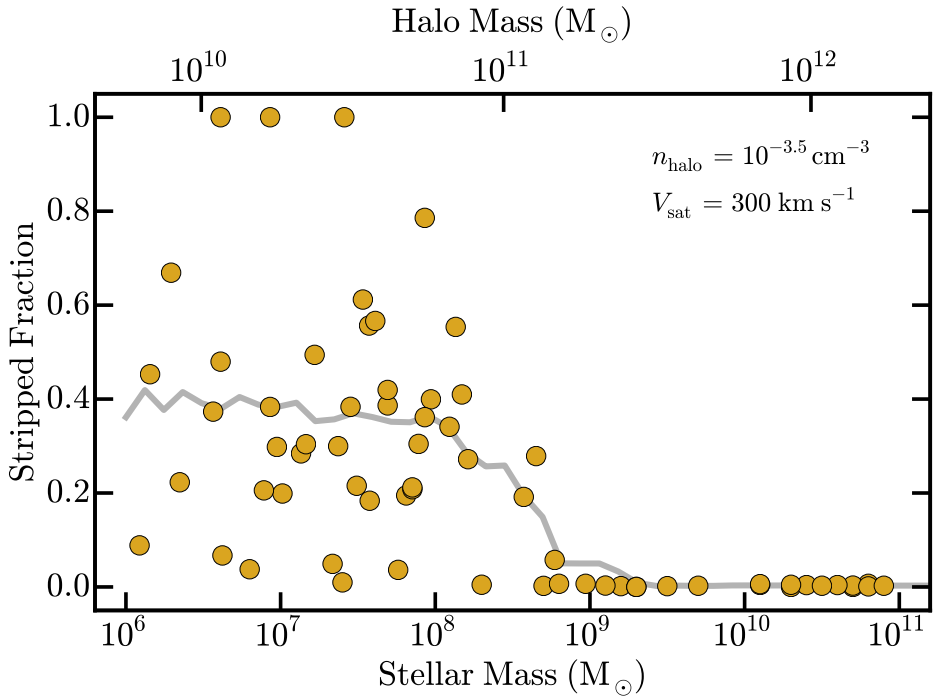

Figure 3.3: The fraction of HI gas stripped ($f_{\rm stripped}$) via ram pressure as a function of stellar mass for our sample of 66 dwarf galaxies, assuming a host halo gas density of $n_{\rm halo} = 10^{-3.5}$ cm^{-3} and a satellite velocity of $V_{\rm sat} = 300$ km s^{-1}. The grey solid line corresponds to the mean $f_{\rm stripped}$ computed in a sliding bin of width 0.6 dex in stellar mass. At stellar masses greater than roughly 10^9 M$_\odot$, we find that satellite systems are unaffected by ram pressure in a Milky Way-like environment. At M$_\star \lesssim 10^{8.5}$ M$_\odot$, however, ram pressure is increasingly effective, with infalling systems typically having $\sim 40\%$ of their cold gas stripped. It is worth noting that the scatter in the stripped fraction at fixed stellar mass is driven entirely by the variation in the HI surface density profiles. For reference, we include the corresponding halo mass for each system, as inferred via the stellar mass-halo mass relation of **?**].

Ram-Pressure Stripping

First, the satellite experiences ram pressure stripping, which is generally assumed to coincide with either initial infall or pericentric passage. As discussed in Section 3.2.1, Equation 3.3 specifies the radial distance, measured from the center of each satellite, at which ram pressure exceeds the gravitational restoring pressure ($R_{\rm strip}$). By integrating the HI surface density profile beyond this radius, we compute the fraction of gas stripped from each satellite as

$$f_{\rm stripped} = \frac{\int_{R_{\rm strip}}^{R_{\rm max}} \Sigma_{\rm gas}(r)\, r\, {\rm d}r}{\int_{0}^{R_{\rm max}} \Sigma_{\rm gas}(r)\, r\, {\rm d}r}\,, \tag{3.7}$$

where $R_{\rm max}$ is the outermost radial distance at which HI is detected. Here, the numerator corresponds to the gas mass that is stripped from the satellite after it interacts with the CGM of the host. The denominator is the total gas mass that resides in the system in the absence of any environmental effects (i.e. prior to infall). The stripped fraction in this scenario is the amount of gas removed in a single, instantaneous interaction between the infalling satellite and the host halo.

As discussed in Section 3.2.3, the adopted definition for $R_{\rm max}$ leads to an underestimate of the stripped fraction, as low-density gas at large galactocentric radii is unaccounted for in our analysis. However, given the sensitivities of the THINGS, Little THINGS, and SHIELD HI maps, any HI component at large radii contributes minimally to the total atomic gas mass, such that the resulting impact on $f_{\rm stripped}$ should be negligible.

Turbulent Viscous Stripping

After estimating $f_{\rm stripped}$ as a result of ram-pressure stripping, we compute the corresponding fraction of gas removed due to turbulent viscous stripping over a maximum timespan of 1 Gyr. First, we test whether the ISM and CGM interface conditions located at $R_{\rm strip}$ are

susceptible to viscous stripping via Equation 3.5. If true, we determine the gas mass lost during a 100 Myr interval, $M_{\rm viscous}$, using Equation 3.6. $M_{\rm viscous}$ is then uniformly removed from the outermost regions of the HI surface density profile, leading to a new $R_{\rm strip}$ in addition to a new value of both $\bar{\rho}_{\rm gas}$ and M_0. The ISM-CGM conditions are then reevaluated allowing the gas removal process to continue if Equation 3.5 is still true. We repeat this process for up to 1 Gyr, leading to a total gas mass lost via turbulent viscous stripping. This additional gas mass is added to the gas which was initially removed via ram pressure to get a total gas mass lost as a result of stripping.

We limit the timespan on which turbulent viscous stripping occurs, so as to roughly match the measured quenching timescale for Local Group satellites [i.e. $\lesssim$ 2 Gyr, **?**]. Approximately 50% (or 55%) of the subhalo population in ELVIS reaches pericenter (or 0.5 $R_{\rm vir}$) within $\sim$ 1.5 Gyr (or $\sim$ 1 Gyr) of infall, where instantaneous ram-pressure stripping is assumed to occur. A further 1 Gyr of turbulent viscous stripping therefore yields a typical quenching time (relative to infall) in rough agreement with the expectations of **?**] and **?**].

3.3 Results

In Figure 3.3, we show the fraction of HI gas ram-pressure stripped from our sample of star-forming galaxies (with no viscous stripping), assuming a host halo density of $n_{\rm halo} = 10^{-3.5}$ cm^{-3} and a satellite velocity of $V_{\rm sat} = 300$ km s^{-1}. For satellite systems with stellar masses greater than $\sim$ 10^9 M$_\odot$, ram pressure is unable to strip the interstellar medium, consistent with the long quenching timescales inferred by **?**] and **?**] at this mass regime. At M$_\star \sim 10^{8-9}$ M$_\odot$, however, we find that ram pressure begins to overcome the local gravitational restoring force, such that a significant fraction of the cold gas reservoir is removed from a typical infalling satellite at M$_\star < 10^8$ M$_\odot$ ($< f_{\rm stripped} > \sim$ 40%). While there is considerable scatter in the efficacy of ram-pressure stripping at low masses, our fiducial model

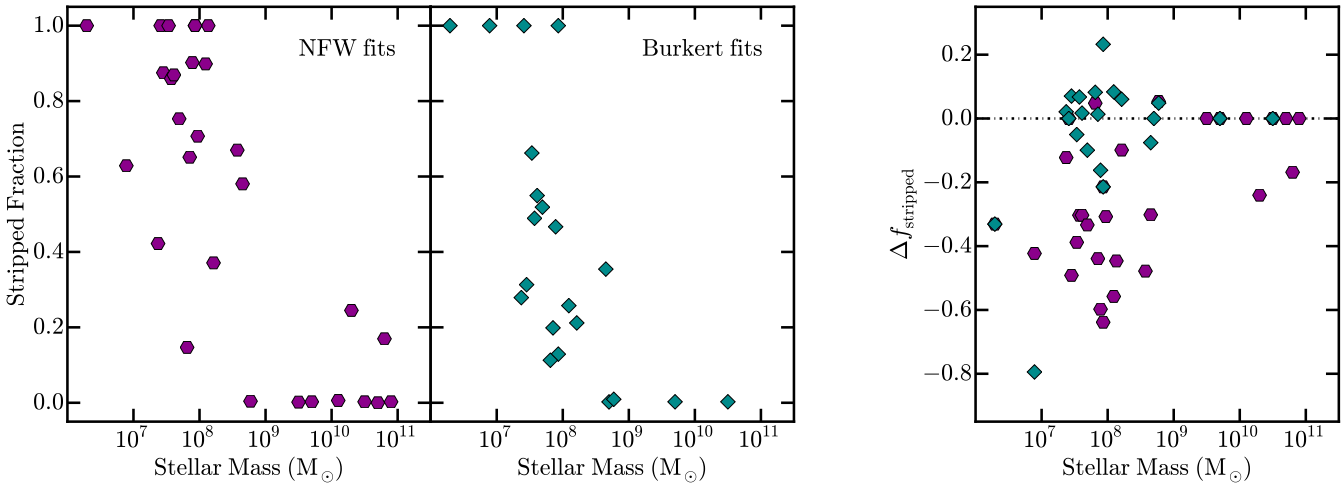

Figure 3.4: (*Left*): the fraction of HI gas ram-pressure stripped ($f_{\rm stripped}$) as a function of stellar mass for the subset of systems with mass profiles determined via dynamical fits to an NFW profile [**?** **?**] and to a Burkert profile [**?**]. As in Fig. 3.3, we assume a halo gas density of $n_{\rm halo} = 10^{-3.5}$ cm^{-3} and a satellite velocity of $V_{\rm sat} = 300$ km s^{-1}. (*Right*): the difference in the fraction of HI gas stripped relative to the corresponding result (see Fig. 3.3) assuming our fiducial mass profile inferred via the stellar mass-halo mass relation of **?**]): $\Delta f_{\rm stripped} = f_{\rm stripped,fid} - f_{\rm stripped,dyn}$. In general, the mass profiles inferred from dynamical modeling favor cored halos, such that stripping is more efficient relative to our fiducial model. Moreover, while there is significant scatter from galaxy to galaxy based upon the assumed mass profile, the qualitative results are universal with ram-pressure stripping becoming increasingly effective at M$_\star < 10^{8-9}$ M$_\odot$.

for a Milky Way-like system qualitatively reproduces the critical mass scale for quenching at $\sim 10^8$ M$_\odot$, such that ram-pressure stripping is a viable candidate to be the dominant quenching mechanism at low satellite stellar masses. In Section 3.3.1 and 3.3.2, we explore how this result depends on the specific parameters adopted in our fiducial model (i.e. $M(r)$, $n_{\rm halo}$, and $V_{\rm sat}$). Additionally, in Section 3.3.3, we discuss how the inclusion of turbulent viscous stripping impacts these results.

3.3.1 Dependence on $M(r)$

The assumed dark matter density profile for each galaxy in our sample is critical in determining the strength of the local gravitational restoring pressure (see Eq. 3.2) and thus the

degree to which ram pressure is able to strip the infalling satellite's ISM. In our fiducial model, the mass profiles, $M(r)$, are determined using the stellar mass-halo mass (SMHM) relation of **?**], assuming an NFW density profile. At low masses, however, less-cuspy dark matter profiles are typically favored and there are large uncertainties in the slope of the stellar mass-halo mass relation (and its scatter, **?**).

To explore how our estimates of $f_{\rm stripped}$ depend on the assumed mass profile, $M(r)$, we utilize alternative mass profiles derived from dynamical fits to the observed HI kinematics for a subset of the systems in our sample. In particular, we utilize the NFW fits to the THINGS and Little THINGS velocity fields from **?**] and **?**], respectively. For 21 galaxies, we also employ Burkert profile fits to the HI kinematics from **?**].

The two left most panels of Figure 3.4 show the fraction of atomic gas stripped for the subset of objects with dynamical mass estimates, assuming a host halo density of $n_{\rm halo} = 10^{-3.5}$ cm^{-3} and a satellite velocity of $V_{\rm sat} = 300$ km s^{-1}. Qualitatively, the dependence of $f_{\rm stripped}$ on satellite stellar mass is very similar to that shown in Fig. 3.3 for our fiducial model, which employs mass profiles inferred from the SMHM relation of **?**]. At $M_\star < 10^{8-9}$ $M_\odot$, ram-pressure stripping becomes increasingly effective. However, the stripped fractions calculated using the dynamical mass profile fits are, on average, slightly greater relative to those produced by our fiducial model. This effect is evident in the far right panel of Figure 3.4, which shows the difference in the stripped fraction for each object as we vary the restoring mass profile. For the dynamical fits to an NFW and Burkert profile (magenta hexagons versus cyan diamonds), we find a mean difference in $f_{\rm stripped}$ of -0.32 and -0.15, respectively. On average, the dynamical fits lead to greater stripped fractions, consistent with these objects being hosted by less-concentrated (or lower-mass) dark matter halos at fixed stellar mass. While there is not perfect agreement between the different halo mass estimators, by adopting the SMHM relation as our fiducial method, we are likely underestimating the stripped fraction and thus providing a conservative estimate of the

effectiveness of ram-pressure stripping.

3.3.2 Dependence on $n_{\rm halo}$ and $V_{\rm sat}$

In addition to the uncertainty in the restoring mass profile, the amount of cold gas stripped from each dwarf is highly dependent on the properties of the host system (i.e. $n_{\rm halo}$ and $V_{\rm sat}$). The density of the host gas halo, for the Local Group in particular, is relatively poorly constrained. To explore how variation in these global parameters will impact our results, we measure the stripped fraction for our sample while varying both the satellite velocity, $V_{\rm sat} = \{200, 250, 300\}$ km s^{-1}, and the density of the halo gas, $n_{\rm halo} = \{10^{-4.0}, 10^{-3.5}\}$ cm^{-3}.

Figure 3.5 shows the mean and 1σ scatter in the stripped fraction as a function of satellite stellar mass for the adopted variation in both the density of the CGM and the satellite velocity relative to the frame of reference of the host. Across the entire range of $V_{\rm sat}$ and $n_{\rm halo}$ explored, ram-pressure stripping becomes effective at roughly the same critical mass scale (10^{8-9} M$_\odot$). The efficacy of ram-pressure stripping at low masses, however, is highly dependent on the chosen parameters for $n_{\rm halo}$ and $V_{\rm sat}$. For example, at M$_\star < 10^9$ M$_\odot$, the stripped fraction decreases, on average, by ~ 0.15 as the satellite velocity is reduced from 300 to 200 km s^{-1} at fixed $n_{\rm halo}$. Similarly, decreasing the host halo density from $n_{\rm halo} = 10^{-3.5}$ cm^{-3} to 10^{-4} cm^{-3} yields an average reduction in $f_{\rm stripped}$ of ~ 0.2 at fixed $V_{\rm sat}$. The scatter in $f_{\rm stripped}$ associated with variation in $V_{\rm sat}$ is particularly noteworthy, given that in our analysis we adopt a single value of $V_{\rm sat}$ for the entire satellite population, thereby neglecting objects that have velocities greater (or less) than this value. At pericentric passage, for example, roughly 60% of subhalos in ELVIS have velocities greater than 300 km s^{-1}. This fraction increases to 82% and 96% for $V_{\rm sat}$ values of 250 and 200 km s^{-1}, respectively.

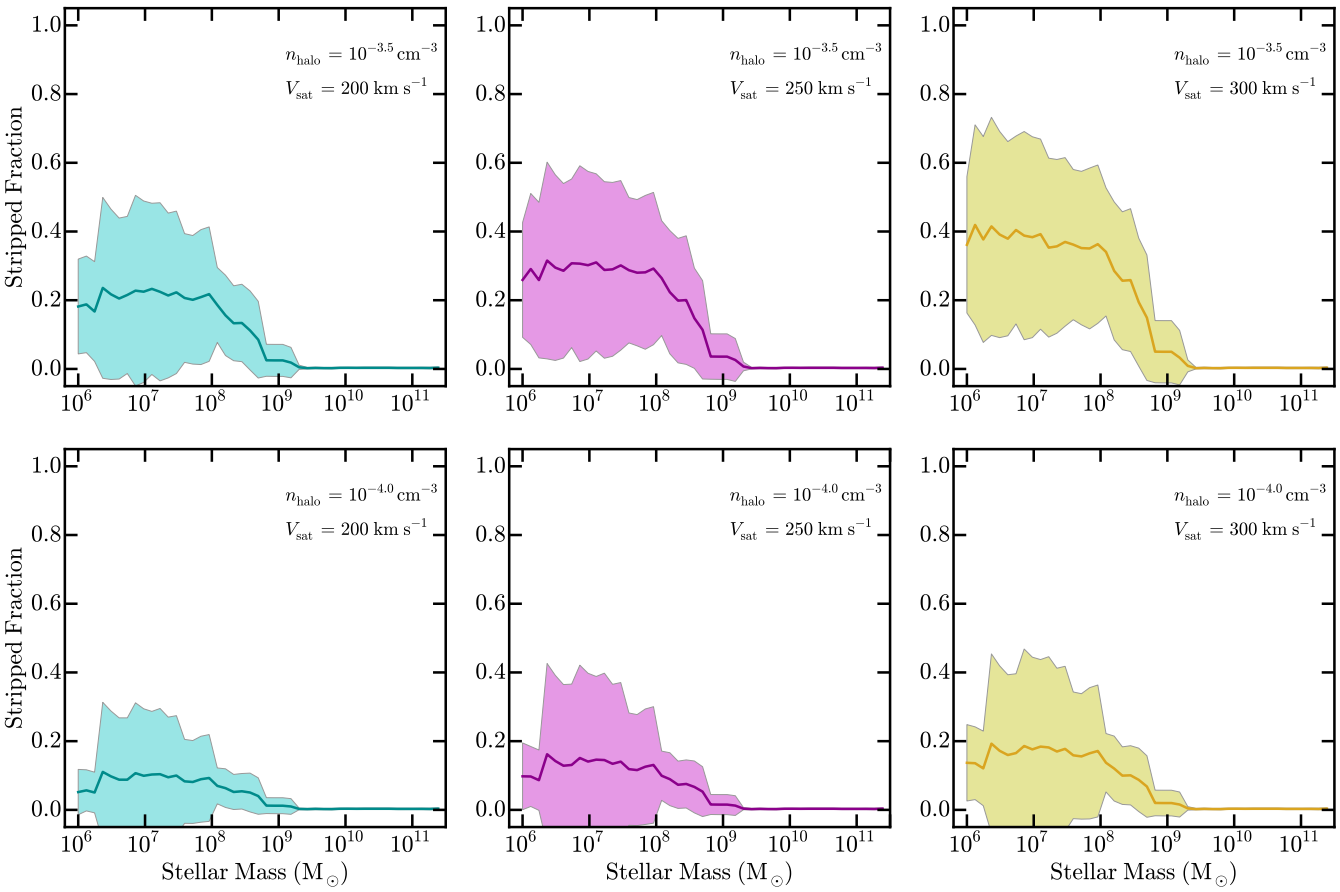

Figure 3.5: The fraction of HI gas stripped ($f_{\rm stripped}$) via ram-pressure stripping as a function of satellite stellar mass for our sample of 66 dwarf galaxies. The solid line in each panel gives the mean $f_{\rm stripped}$ in a sliding bin of width 0.6 dex in stellar mass, with the shaded region tracing the corresponding 1σ scatter. In the *top* and *bottom* rows, we assume a host halo gas density of $n_{\rm halo} = 10^{-3.5}$ cm^{-3} and $10^{-4.0}$ cm^{-3}, respectively. From *left* to *right*, the satellite velocity varies from 200 (cyan) to 250 (magenta) to 300 km s^{-1} (gold). While the efficiency of ram-pressure stripping depends on the assumed properties of the host halo, such that $< f_{\rm stripped} >$ ranges from $\sim 10 - 40\%$, the satellite stellar mass where ram-pressure stripping becomes significant is universally $< 10^9$ M$_\odot$.

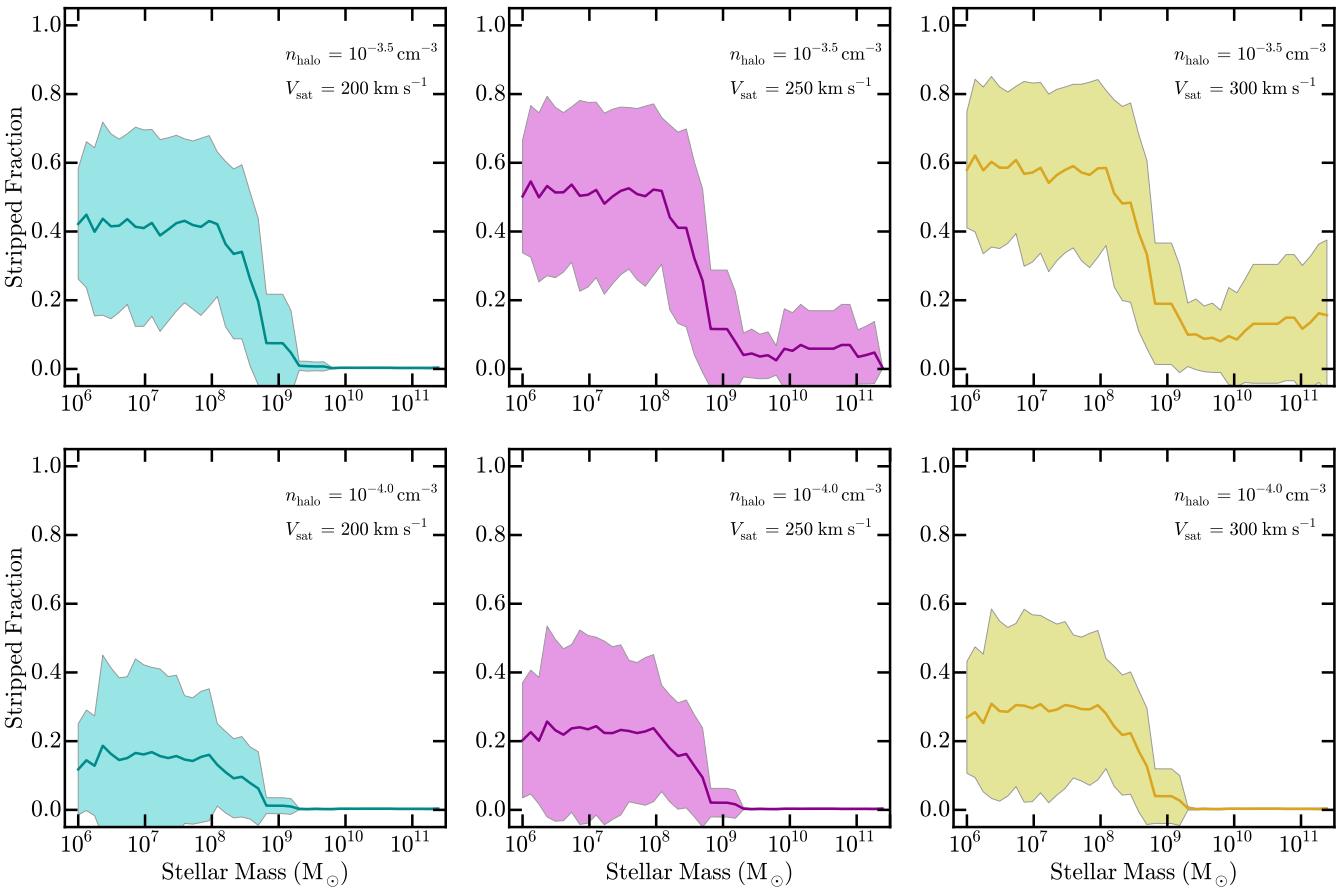

Figure 3.6: The fraction of HI gas stripped ($f_{\rm stripped}$) via ram-pressure *and* turbulent viscous stripping as a function of satellite stellar mass for our sample of 66 dwarf galaxies. The solid line in each panel gives the mean $f_{\rm stripped}$ in a sliding bin of width 0.6 dex in stellar mass, with the shaded region tracing the corresponding 1σ scatter. In the *top* and *bottom* rows, we assume a host halo gas density of $n_{\rm halo} = 10^{-3.5}$ cm^{-3} and $10^{-4.0}$ cm^{-3}, respectively. From *left* to *right*, the satellite velocity varies from 200 (cyan) to 250 (magenta) to 300 km s^{-1} (gold). Including both ram-pressure and turbulent viscous stripping, we find an increase in the fraction of stripped gas, such that the majority of gas is removed from low-mass satellites orbiting hosts with a halo gas density of $10^{-3.5}$ cm^{-3}.

3.3.3 Turbulent Viscous Stripping

While ram-pressure stripping is effective at removing gas from satellites below the critical quenching mass scale ($\lesssim$ 10^8 $M_\odot$), it is only able to strip roughly half of the cold gas reservoir on average. As discussed in Section 5.1, however, infalling satellite systems are also subject to turbulent viscous stripping, which results from K-H instabilities at the interface of the satellite's ISM and the CGM. To estimate the impact of this secondary stripping mechanism, we allow turbulent viscous stripping to proceed for up to 1 Gyr following the initial ram-pressure stripping.

Figure 3.6 shows the mean and 1σ scatter in the stripped fraction due to both ram-pressure *and* turbulent viscous stripping as a function of satellite stellar mass, assuming the same range of $V_{\rm sat}$ and $n_{\rm halo}$ values as in Figure 3.5. In contrast to when ram-pressure acts alone, the inclusion of turbulent viscous stripping at high satellite velocities ($V_{\rm sat} \geq 250$ km s^{-1}) and host halo densities ($n_{\rm halo} \geq 10^{-3.5}$ cm^{-3}) yields non-zero stripped fractions for some massive satellites. As discussed in Section 4.4, the amount of gas removed, however, is relatively modest ($< f_{\rm stripped} > \lesssim 0.2$), in agreement with the observations of massive satellites in the Local Group. At low stellar mass, the efficacy of stripping is notably increased when including turbulent viscous effects, such that the typical stripped fraction is roughly 1.5$\times$ that produced by ram-pressure stripping alone. For a host halo density of $n_{\rm halo} = 10^{-3.5}$, the majority of satellites in our sample are stripped of more than half of their cold gas reservoirs.

3.4 Discussion

Recent studies of satellite galaxies in the local Universe find that the efficiency of satellite (or environmental) quenching – or the timescale upon which it occurs following infall – strongly depends on the mass of the satellite system [**? ? ? ? ?**]. For satellites with $M_\star \gtrsim 10^8$ $M_\odot$,

the long quenching timescales inferred from the relatively low observed satellite quenched fractions are consistent with starvation as the dominant quenching mechanism [**?** , see also **?**]. At stellar masses below a critical mass scale of $M_\star \lesssim 10^8$ $M_\odot$, however, the lack of quenched systems in the field combined with the very high satellite quenched fractions observed in the Local Group require a very short quenching timescale, consistent with a physical process that acts on roughly the dynamical time, such as ram-pressure stripping [**?** **?**]. While stripping, and in particular ram-pressure stripping, is often thought to be a possible factor in the dearth of star-forming dwarfs in the Local Group [**?** **?** **?**], these recent results provide possible benchmarks by which to measure stripping as an active quenching mechanism. In particular, does stripping become dominant at $M_\star \lesssim 10^8$ $M_\odot$, and is it strong enough to quench low-mass satellites on a timescale of ~ 2 Gyr in host systems such as the Milky Way or M31?

3.4.1 Reproducing the Critical Mass Scale for Satellite Quenching

As first shown by **?** , see also **?** **?**], observations of galaxies in the Local Volume point towards a remarkable shift in the efficiency of satellite quenching below a satellite stellar mass of $\sim 10^8$ $M_\odot$, such that quenching at low masses proceeds relatively quickly following infall. Recent analysis of much larger samples of Milky Way-like hosts in deep photometric datasets support this picture (Phillips et al. in prep), indicating a global critical mass scale for satellite quenching. In agreement with this picture, we find that ram pressure begins to overcome the local gravitational restoring force only in systems below a stellar mass of $\sim 10^9$ $M_\odot$. Above this mass scale, dwarfs are largely resistant to ram-pressure stripping, consistent with inefficient quenching via starvation. At low masses, however, ram-pressure stripping is able to remove (at least some of) the fuel for star formation from an infalling satellite system, thus contributing to quenching and potentially driving the change in quenching efficiency below $\sim 10^8$ $M_\odot$. Moreover, when including turbulent viscous stripping, this critical scale

for satellite quenching persists, with a dramatic increase in stripping efficiency evident over the full range of $n_{\rm halo}$ and $V_{\rm sat}$ values explored. Altogether, our results show that stripping naturally gives rise to a critical scale for satellite quenching, consistent with observations in the local Universe.

Unlike ram pressure, we find that at high halo densities and satellite velocities turbulent viscous stripping is able to remove cold gas from some infalling satellites in the high-mass regime (i.e. $> 10^9$ $M_\odot$). The amount of gas removed, however, is relatively modest and in broad agreement with observations of massive satellites in the Local Group. For example, there is clear evidence for stripping of the LMC and SMC, which are the only Milky Way satellites more massive than 10^8 $M_\odot$. However, the stripped gas that comprises the Magellanic Stream and Leading Arm [**?**], may result from tidal effects [e.g. **? ? ? ?**] versus ram-pressure or viscous stripping [e.g. **? ? ? ?**]. Given the uncertainties associated with the orbit of the LMC and SMC and the physical origins of the stripped gas, it is difficult to make a clear accounting of the stripped fraction for the two systems [e.g. **?**]. However, the total HI gas mass attributed to the Magellanic Stream and Leading Arm versus that of the two Magellanic Clouds jointly is consistent with an average stripped fraction for the two systems of $\lesssim 25\%$, consistent with our expectations at $M_\star > 10^8$ $M_\odot$ [see Fig. 3.6, **? ? ?**].

Finally, the mass scale at which stripping begins to be effective should depend directly on the the properties of the host system (i.e. $n_{\rm halo}$ and $V_{\rm sat}$ in our analysis). That is, these parameters should, on average, scale with the mass of the host, such that a typical infalling satellite would experience a stronger ram pressure in more massive host systems and the critical mass scale for satellite quenching would increase accordingly. While values of $n_{\rm halo}$ and $V_{\rm sat}$ consistent with those expected for the Milky Way lead to an onset of stripping at roughly $\sim 10^{8-9}$ $M_\odot$, observations of more massive host systems, such as rich groups and clusters, should yield high quenched fractions at yet higher masses as the critical quenching mass increases with host mass. This picture is supported by observations of local clusters,

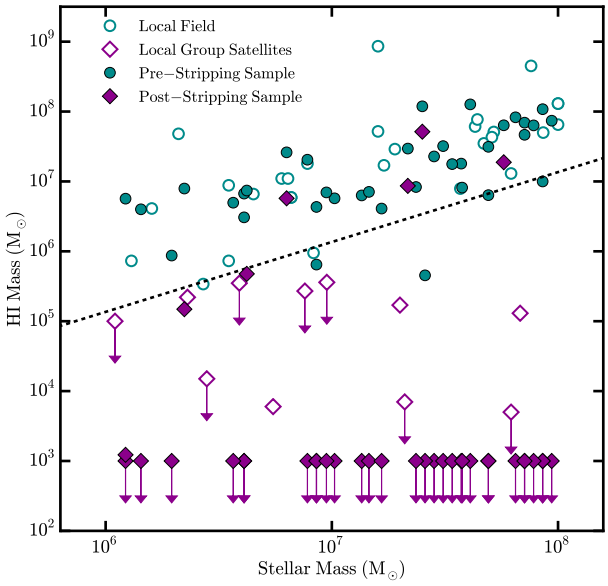

Figure 3.7: The HI gas mass as a function of stellar mass for our galaxy sample at $M_\star < 10^8$ $M_\odot$, prior to infall (solid cyan circles) and after interaction with the host CGM (solid magenta diamonds). To account for potential variations in the local halo gas density, we assume $n_{\rm halo} = 10^{-3}$ cm^{-3} and $V_{\rm sat} = 300$ km s^{-1}, including both ram pressure and turbulent viscous effects in our stripping calculations. For comparison, we show the observed HI gas masses for field galaxies in the Local Volume (open cyan circles) and satellites of the Local Group (open magenta diamonds) from **?**] and **?**]. Arrows indicate observed upper-limits or systems that are completely stripped in our analysis. The dashed black line corresponds to an HI gas fraction of 0.136, below which we define a galaxy as quenched. Including a clumpy host CGM, we find that stripping is able to quench $\sim 90\%$ of our infalling satellite population at low masses (33 out of 37 systems).

which find very few star-forming satellites at stellar masses of $10^{9.5}$ $M_\odot$ versus the $\sim 30\%$ quenched fraction measured for group and Milky Way-like hosts [e.g. **? ? ? ?**].

3.4.2 Does Stripping Quench Low-Mass Satellites?

While ram-pressure stripping acts at the correct mass scales, our analysis finds that ram pressure alone is unable to suppress star formation in infalling satellites on the timescales predicted by **?**]. As shown in Fig. 3.5, for expected values of $n_{\rm halo}$ and $V_{\rm sat}$, infalling satellites are typically ram-pressure stripped of $< 50\%$ of their cold gas reservoirs. Given the typical

HI gas fractions and star formation rates for low-mass field dwarfs, which imply exceptionally long depletion timescales [**?** **?** **?**], a satellite stripped of only 50% of its cold gas will still retain enough fuel to potentially form stars for many Gyr. For $n_{\rm halo} = 10^{-3.5}$ cm^{-3} and $V_{\rm sat} =$ 300 km s^{-1}, the gas fractions for our satellite population, following ram-pressure stripping, are still typically $\sim 3\times$ greater than the current observational limits for quenched satellites in the Local Group [i.e. $f_{\rm HI} \lesssim 0.136$, **?**]; that is, ram pressure only quenches $\lesssim 15\%$ of our low-mass satellite population, such that $f_{\rm HI} < 0.136$. Ultimately, to reproduce the observed HI gas fractions for satellites in the Local Group and thus the inferred satellite quenching timescales at low stellar masses, ram-pressure stripping would need to be substantially more efficient than our predictions (i.e. stripping nearly the entire cold gas reservoir of all systems, $<f_{\rm stripped}> \sim 0.9$). **?**] come to a similar conclusion based on wind-tunnel modeling of an idealized Leo T-like satellite during infall. Using the FLASH hydrodynamics code [**?**], they find that ram-pressure stripping is unable to fully strip the satellite within 2 Gyr.

With the inclusion of viscous effects in our fiducial model, stripping is able to remove the majority of cold gas from the low-mass, infalling satellite population (i.e. at $\rm M_\star < 10^8\ M_\odot$, see Fig. 3.6). In 60% of low-mass systems following stripping, we find HI gas fractions consistent with the observed limits for the Milky Way dwarf spheroidal population ($f_{\rm HI} < 0.136$), such that stripping is nearly able to reproduce the high satellite quenched fraction observed in the Local Group ($f_{\rm quenched} \sim 0.9 - 1$). For roughly 40% of systems, however, the resulting gas fractions – post stripping – are still greater than that observed for satellites of the Milky Way. Again, to bring our satellite population into agreement with the roughly $90 - 100\%$ satellite quenched fraction at low masses in the Local Group requires yet stronger stripping, such that the typical stripped fraction is closer to $f_{\rm stripped} \sim 0.9$ at $\rm M_\star \lesssim 10^8\ M_\odot$.

While current observations of comparable nearby systems (e.g. M81, M106) find low-mass satellite populations that roughly mirror that found in the Local Group [**?** **?**], it remains possible that the low-mass satellite quenched fractions for the Milky Way and M31 are

abnormally high relative to comparable host halos. As shown in Fig. 3 of **?**], if the satellite quenched fraction for a Milky Way-like halo is typically $\sim 70\%$ (versus $90 - 100\%$), the satellite quenching timescale increases to $\sim 4 - 5$ Gyr (versus $\sim 1 - 2$ Gyr). In such a scenario, stripping would not need to fully quench infalling satellites; instead, stripping could simply remove roughly half of a satellite's cold gas supply, so as to decrease the depletion (i.e. starvation) timescale accordingly. Our analysis suggests that this level of stripping is very much realistic for a Milky Way-like environment, even from ram pressure alone.

3.4.3 The Efficacy of Stripping: Refining Our Analysis

Within our analysis, there are several factors or approximations by which we are likely over- or under-estimating the true effectiveness of stripping. For example, we assume instantaneous ram-pressure stripping, which likely overestimates the ram pressure [**?**]. Moreover, like many studies of ram-pressure stripping, we adopt a smooth host halo in equilibrium with the dark matter potential. X-ray observations, however, find that massive hot halos, typically associated with galaxy clusters, exhibit structure on scales of $\lesssim 1$ Mpc [**?** **?**]. In addition, quasar absorption-line studies of low- and high-z hosts find significant clumpiness in the CGM of massive galaxies [e.g. **?** **?**]. What the observed substructure in these systems implies for a typical Milky Way-like object is unclear, but the assumption of a smooth halo certainly ignores potentially important details. Specifically, a clumpy gas halo will yield regions of higher density and thus an increased ram pressure. Such a halo is also likely to have some net velocity relative to the host's dark matter halo (our point of reference in determining satellite velocities, see Section 3.2.2). As shown by **?**], bulk motion of the gas halo tends to be in the same direction as that of the satellites, leading to a smaller effective $V_{\rm sat}$ and thus weaker ram pressure. Clearly, more detailed hydrodynamical simulations are needed to fully address the impact of a clumpy CGM on our calculations. However, to quench roughly $80 - 90\%$ of satellites in our sample via stripping (i.e. including ram-pressure and

viscous effects) requires local variations in the halo gas density on the order of $2-3\times$ that assumed in our fiducial model (i.e. $n_{\rm halo} = 10^{-3.25} - 10^{-3}$ cm^{-3}), given a satellite velocity of 300 km s^{-1}. As shown in Figure 3.7, by including a clumpy CGM, our analysis is able to reproduce the observed HI gas fractions for the Local Group satellite population, with $\sim 90\%$ of our satellite population quenched following infall. To achieve the same quenched efficiency with a satellite velocity of only 200 km s^{-1}, thereby accounting for potential bulk motion of the halo gas, our analysis requires a local increase in CGM density of roughly $10-20\times$ that of our fiducial model (i.e. $n_{\rm halo} = 10^{-2.5} - 10^{-2.2}$ cm^{-3}). While such extreme CGM densities are unrealistic on average, local variations of this scale are in good agreement with the results of recent hydrodynamic simulations of stripping by **?**], which find that galaxies undergoing stripping in groups and clusters typically experience increased ram pressure associated with CGM overdensities as large as $100\times$ the mean.

Along with potential variations in the density of the host CGM, the efficacy of stripping is also impacted by the density of the satellite dark matter halo. As discussed in Section 3.3.1, the satellite dark matter halo mass profiles assumed in our fiducial model yield a potentially significant underestimate of the stripping efficiency. If low-mass dwarfs live in less-concentrated host halos, as suggested by their observed internal kinematics, the resulting stripped fractions should increase by $\gtrsim 10\%$. With the inclusion of cored mass profiles, stripping becomes an increasingly realistic physical driver for the high quenched fractions and short quenching timescales for low-mass satellites.

While adopting less-concentrated mass profiles alone will likely not be enough to fully strip all systems, it emphasizes another missing ingredient in our analysis: baryonic feedback. As shown by **?**], field dwarfs (and thus infalling satellites) are nearly universally star-forming at stellar masses of $\lesssim 10^9$ M$_\odot$ and will be subject to the stellar feedback associated with radiation pressure and supernovae [e.g **?** **?**]. As part of our analysis, we employ observed HI surface density profiles for a sample of star-forming field dwarfs, along with halo masses

modeled from spatially-resolved kinematics, which should thus naturally capture the impact of feedback on $\Sigma_{\rm gas}$ and $M(r)$. Infalling satellites, however, may experience an elevated level of star formation and thus feedback. This increased star-formation activity would result from compression of the satellite's ISM due to interaction with the host CGM, thereby increasing the local gas density and allowing star formation to proceed at an accelerated rate. For example, simulations of massive satellites in groups and clusters find that ram pressure often leads to a burst of star formation for the infalling system [**?** **?** **?**]. Within the Local Group, modeling of the orbit and star-formation history of Leo I suggest that it experienced a small burst of star formation at pericentric passage prior to being quenched, consistent with being initiated by ram pressure [**?** **?** **?**]. This increase in star formation, driven by interaction with the host CGM, can inject energy into the ISM of the satellite, puffing up the system and thereby making it more susceptible to stripping [**?** **?** , but see also **?**]. High-resolution hydrodynamic simulations of Milky Way- or Local Group-like environments should provide a robust means for studying the possible importance of feedback in increasing the efficiency of stripping (e.g. **?** **?** **?** ; Garrison-Kimmel et al. in prep).

3.4.4 Towards a Complete Picture of Satellite Quenching

Figure 3.8 presents current constraints on the satellite quenching timescale from **?**], **?**], and **?**] along with a qualitative depiction of the dominant quenching mechanisms likely at play as a function of satellite stellar mass. As illustrated by **?**], the measured satellite quenching timescales at high masses, including the lack of strong dependence on host halo mass, are broadly consistent with the expectations for quenching via starvation [see also **?** **?**]. At low masses, on the other hand, the short quenching timescales inferred from analysis of the Local Group satellite population are difficult to fully explain. As our analysis shows, stripping is a likely culprit in suppressing star formation at low masses, as it qualitatively reproduces the critical mass scale for satellite quenching ($M_{\rm crit}$) within the Local Group.

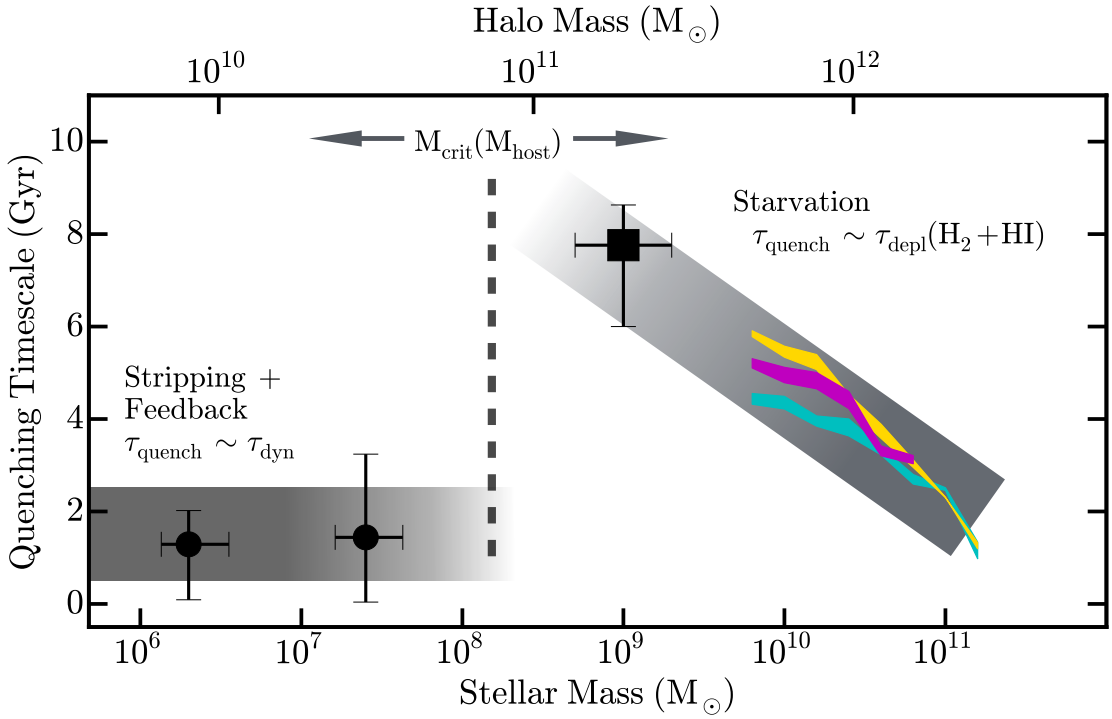

Figure 3.8: The dependence of the satellite quenching timescale on satellite stellar mass in Milky Way-like and more massive host halos ($> 10^{12}$ M$_\odot$), as adapted from **?**]. The magenta, gold, and cyan colored bands show the constraints from **?**] for satellites in host halos of $M_{\rm host} \sim 10^{12-13}$ M$_\odot$, 10^{13-14} M$_\odot$, 10^{14-15} M$_\odot$, respectively. The black square and circles correspond to the typical quenching timescale for intermediate- and low-mass satellites from **?**] and **?**], respectively. The light grey shaded regions highlight the expected dominant quenching mechanism as a function of satellite mass, while the vertical dashed black line denotes the critical mass scale below which satellite quenching becomes increasingly efficient. At M$_\star \gtrsim 10^8$ M$_\odot$, the satellite quenching timescales show broad agreement with the observed gas depletion timescales for field systems, suggesting that starvation is the main driver of satellite quenching at these masses. At low masses, stripping – potentially assisted by stellar feedback and a clumpy host CGM – is the most probable mechanism responsible for the high satellite quenched fractions and short quenching timescales observed in the Local Group. The critical satellite stellar mass, $M_{\rm crit}$, at which the dominant quenching mechanism shifts from starvation to stripping should depend on the halo mass of the host system, with more massive hosts able to strip more massive satellites.

However, our analysis suggests that stripping (and specifically ram-pressure stripping) may require a significantly clumpy host CGM or the assistance of baryonic feedback to effectively remove enough cold gas from the most gas-rich and concentrated systems. Additionally, recent work by **?**] and **?**] shows that the distribution of HI in low-mass field galaxies can be significantly altered via close encounters with neighboring dwarfs. If these encounters occur just before or during infall onto a host system, the resulting satellite's ISM will likely be more susceptible to stripping.

If stripping drives quenching at low masses, then there are clear implications regarding the CGM of the Milky Way and similar systems. In particular, to quench all low-mass satellites within ~ 2 Gyr of infall requires that the CGM extends to roughly 0.5 $R_{\rm vir}$ [or ~ 150 kpc, **?**] at a density of $n_{\rm halo} \gtrsim 10^{-3.5}$ cm^{-3}. This large physical extent is needed to explain the quenching of satellites with more circular or non-plunging orbits. In ELVIS, we find that $\sim 25\%$ of subhalos in our selected mass range and accreted at $0.15 < z_{\rm infall} < 3$ reach their first pericentric passage at $0.5 < R/R_{\rm vir} < 1$. To reproduce the extremely high satellite quenched fractions at $\lesssim 10^8$ M$_\odot$ via stripping, the CGM must therefore have a relatively cored density profile [e.g. **?**].

While the physical picture presented in Fig. 3.8 broadly explains the suppression of star formation in satellite systems, it largely ignores any corresponding structural evolution. Recent observations at intermediate redshift suggest that quenching of massive central galaxies is closely associated with development of a bulge-dominated morphology [**?** **?**]. Moreover, observations of galaxy morphology in field and group/cluster populations at M$_\star \gtrsim 10^{9.5}$ M$_\odot$ point towards an evolution of satellite systems from disk- to bulge-dominated [**?** **?**], suggesting that an additional mechanism beyond starvation must likely be driving satellite evolution — unless fading of the stellar population, post quenching, can account for observed differences in the light profiles of field and satellite populations. In lower-mass hosts such as the Milky Way, however, there is little morphological difference between massive satellites and

field systems of comparable mass [**?**]. In addition, at lower satellite masses, structural evolution of satellites is relatively modest following infall and is potentially driven by baryonic feedback effects [**?** **?**].

3.5 Summary

Through the utilization of observed HI surface density profiles for nearby dwarf galaxies, we investigated the effectiveness of ram-pressure and turbulent viscous stripping in Milky Way-like environments. Our analysis was motivated by recent results which point towards a sharp change in the satellite quenching timescale, and therefore the dominant quenching mechanism, for low-mass satellite galaxies. The principal results of our analysis are as follows:

- Ram-pressure and turbulent viscous stripping become increasingly effective in satellite galaxies with $M_\star \lesssim 10^9\ M_\odot$, consistent with the observed decrease in the satellite quenching timescale at $M_\star \sim 10^8\ M_\odot$. If stripping dominates the quenching of low-mass satellites, then we predict that the critical mass scale for satellite quenching should increase with host halo mass.

- Assuming a smooth host halo with a density of $n_{\rm halo} = 10^{-3.5}$ cm^{-3} and a satellite velocity of $V_{\rm sat} \sim 300$ km s^{-1}, we find that stripping is able to remove enough cold gas so as to quench $\sim 60\%$ of infalling satellites at low masses. However, when including a clumpy halo, such that the typical CGM density at which stripping occurs is $n_{\rm halo} \sim 10^{-3.25} - 10^{-2.5}$ cm^{-3} (i.e. $\sim 2 - 20$ times the mean density), stripping is able to effectively quench $\sim 90\%$ of infalling satellites, such that their gas fractions agree with observational limits for dwarf spheroidals in the Local Group.

- The efficiency of stripping may be further enhanced with the inclusion of stellar feedback, which could play an important role in making satellite systems susceptible to ram pressure and turbulent viscous effects. Further studies of stripping via hydrodynamic simulations will be a critical step in further constraining the role of stripping in the quenching of low-mass satellites.

Chapter 4

Environmental Quenching of Low-Mass Field Galaxies

4.1 Introduction

Recent observations of nearby dwarf galaxies show that low-mass systems ($M_\star \lesssim 10^9$ $M_\odot$) currently residing > 1 Mpc from a massive neighbor are almost exclusively star forming [**? ? ? ?**]. This is supported by HI observations of systems in the Local Volume, which find a predominately gas-rich field population [**?**]. Together, these results indicate that low-mass systems largely lack the ability to cease forming stars, or quench, in the field. In other words, "*in situ*" processes, such as morphological quenching [**?**] or stellar feedback [**? ?**] that operate on more massive field galaxies appear unable to shut down star formation at the lowest galaxy masses.

In contrast to the local field population, the low-mass satellites of the Local Group are nearly universally quenched [e.g. **? ? ?**]. This dramatic difference in the star-forming properties of low-mass field and satellite galaxies strongly indicates that environmental mechanisms are

responsible for quenching low-mass systems. Moreover, the environmental mechanism at play must act with great efficiency [i.e. rapidly following infall, **?** **?**]. Using N-body simulations to model the accretion history of satellites in the Local Group, **?**] present a coherent picture of satellite quenching as a function of satellite and host mass in which satellites above a host-dependent, critical mass scale are quenched via starvation while low-mass systems are rapidly quenched via stripping. This model is supported by complementary observations of satellite populations in the local Universe, such that it reproduces the fraction of quenched satellites at $z \sim 0$ over a broad range of masses [e.g. **?** **?** **?** **?**].

Studies of dark matter halo populations within N-body simulations, however, show that a significant fraction of low-mass halos residing just beyond the virial radius ($R_{\rm vir}$) of a massive halo today were previously located within $R_{\rm vir}$ [**?** **?** **?** **?** **?**]. For example, **?**] find that these so-called "backsplash" halos comprise roughly 50% of systems in the Local Volume (i.e. within $1 < R/R_{\rm vir} < 2$ of the Milky Way). Given this sizable backsplash population, highly-efficient satellite (or environmental) quenching, needed to reproduce the Local Group satellite population at low masses, could be expected to produce a non-negligible number of quenched galaxies in the field — potentially in conflict with current observations.

In this work, we utilize a suite of N-body simulations to investigate the degree to which environmental quenching models reproduce the observed population of quenched field galaxies that are currently known to reside beyond the virial radius of either the Milky Way or M31 (i.e. in the Local Volume). Specifically, does the model of satellite quenching presented by **?** **?**] overproduce the relative number of quenched systems in the field? For more massive galaxies ($\sim 10^{9.5}$ $M_\odot$), where environmental quenching is less efficient, **?**] show that observations agree with the expectations of the model, with $\sim 40\%$ of systems within ~ 2 $R_{\rm vir}$ of local groups and clusters likely quenched by environmental effects. In Section 4.2, we detail the observational and simulation data used in this analysis. Additionally we introduce the quenching models that facilitate comparison between observations and theory. In

Section 4.3 and 4.4, we present our results and discuss any implications and limitations this analysis might have on the current galaxy evolution paradigm. Finally, in Section 4.5, we summarize this work and discuss how ongoing efforts will clarify and enhance this framework of environmental quenching of dwarf satellite galaxies. Where necessary, we adopt a ΛCDM cosmology with the following parameters: $\sigma_8 = 0.801$, $\Omega_{\rm m} = 0.266$, $\Omega_\Lambda = 0.734$, $n_{\rm s} = 0.963$, and $h = 0.71$ [WMAP7, **?**].

4.2 Data and Models

4.2.1 Local Volume Dwarfs

Our sample of local dwarf galaxies is drawn from the compilation of **?**]. The dataset builds upon the low-mass satellite sample from **?**] by extending beyond the virial radius of the Milky Way and M31 systems while maintaining the same stellar mass range in order to facilitate a clean comparison to the known classical satellites of the Local Group. Our field population is selected to be in the stellar mass range $\sim 10^6 - 10^8$ $M_\odot$ and within 1.2 Mpc of either the Milky Way or M31. While this stellar mass range leads to a complete sample of dwarf galaxies inside the virial radius of the Milky Way and out to 0.5 $R_{\rm vir}$ in M31, the field sample within the Local Volume is potentially incomplete at these stellar masses.

?] demonstrate that all-sky surveys using photographic plates are complete down to a surface brightness of ~ 25.5 mag arcsec^{-2}. This roughly corresponds to And V ($M_\star \sim 4 \times 10^5$ $M_\odot$) at the distance of M31, suggesting that we are largely complete for stellar masses above a few $\times$ 10^5 $M_\odot$ out to distances of at least $\sim$ 750 kpc from the Milky Way. Inside the footprints of the Sloan Digital Sky Survey [**?**] and the Dark Energy Survey [**? ?**], however, dwarf galaxy samples are complete well below our lower stellar mass limit of $M_\star = 10^6$ $M_\odot$ out to distances of (at least) 1.5 Mpc from the Milky Way [**? ? ? ? ?**]. Finally, while

all optical imaging datasets will suffer incompleteness due to obscuration by the disk of the Milky Way, assuming the dwarf galaxy population is not biased in a manner where quenched (or star-forming) objects preferentially reside behind the disk, our results should not be strongly affected by this incompleteness.

Our final sample includes 11 dwarf galaxies in the field within 1.2 Mpc in addition to the previously-identified 12 satellite galaxies from **?**]. The left-hand panel of Figure 4.1 shows the host-centric radial velocities for our sample [**?** **?** **?**], scaled by $\sqrt{3}$ to approximately account for tangential motion, as a function of distance to the nearest host (Milky Way or M31). The vertical dotted line at 300 kpc denotes the approximate location of the virial radius in a Milky Way-like dark matter halo. Throughout this work, we adopt $R_{\rm vir} = 300$ kpc for both the Milky Way and M31. The dashed lines illustrate the region in which a subhalo is likely bound to the host, assuming a Navarro-Frenk-White (NFW) dark matter halo profile [**?**] with a virial mass of 2×10^{12} $M_\odot$ and a concentration of 8.

In the right-hand panel of Figure 4.1, we show the HI gas fraction for each dwarf in our sample as a function of host-centric distance. The filled points correspond to HI detections while the open points denote upper limits [**?** **?** **?**]. To separate gas-rich, star forming systems from gas-poor, quenched systems, we divide the sample based on the HI gas fraction ($M_{\rm HI}/M_\star$). Galaxies with an HI gas fraction above 0.2 are considered star forming, while galaxies with HI gas fractions below 0.2 are quenched. The points in Fig. 4.1 are color-coded according to this classification, with blue and red points corresponding to star forming and quenched dwarfs, respectively. Our resulting quenched fraction in the local field is $f_{\rm quench} = 0.36 \pm 0.15$, assuming a binomial error on the measured quenched fraction. The measured quenched fraction is largely independent of host-centric distance, with $f_{\rm quench} = 0.40 \pm 0.22$ within $1 < R/R_{\rm vir} < 2$ and $f_{\rm quench} = 0.33 \pm 0.19$ within $2 < R/R_{\rm vir} < 4$, which suggests that our sample is not dramatically incomplete for passive systems at large distances. While varying the classification threshold for quenched versus star-forming systems will have a mild impact

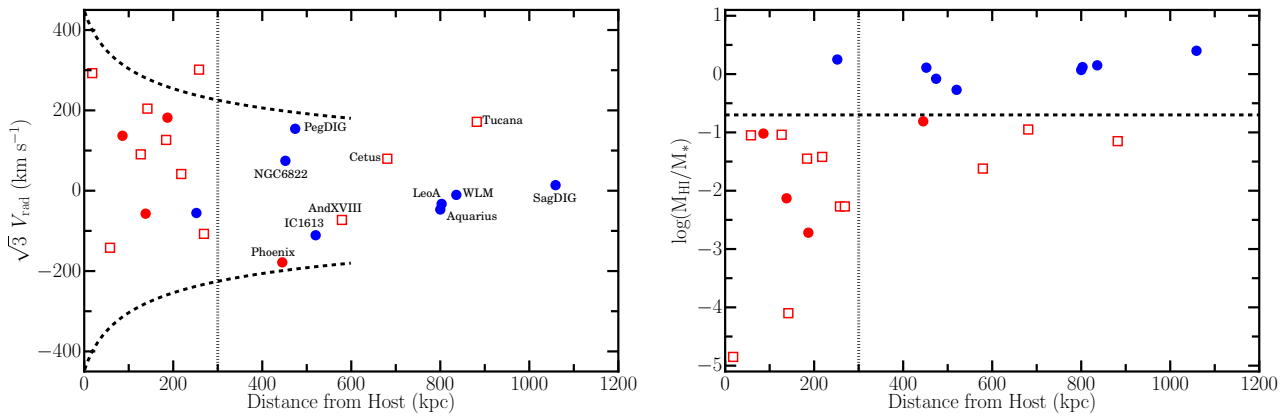

Figure 4.1: *Left*: Host-centric radial velocity (scaled by $\sqrt{3}$ to approximately account for tangential motion) for all known Local Volume dwarf galaxies in the stellar mass range $10^6 - 10^8$ M$_\odot$ as a function of distance from the nearest host (either the Milky Way or M31). The dotted vertical line roughly corresponds to the virial radius of a Milky Way-like host and the dashed lines correspond to the boundary between bound and unbound systems. Satellite points are color-coded according to their observed HI gas fraction, with blue (and red) points denoting gas-rich (and gas-poor) systems, respectively. The closed points signify HI detections, while the open points correspond to upper limits on the total HI mass. *Right*: The gas fraction ($M_{\rm HI}$/M$_\star$) as a function of distance from the nearest host for the same dwarf galaxies as in the left panel. The horizontal dashed line corresponds to a gas fraction of 0.2, below which systems are considered quenched.

on the measured quenched fraction, it does not significantly change the qualitative results of this analysis.

As an independent measure of the quenched fraction, we also include data from the Updated Nearby Galaxy Catalog [UNGC, **?**]. Objects are selected according to the same stellar mass limits ($10^6 - 10^8$ $M_\odot$), given their K-band magnitude and assuming a mass-to-light ratio of $M/L = 1$ [**?**]. Due to the heterogeneity of star formation rate measurements within the UNGC, we instead use the morphology of each system as an indicator of its current star-forming activity. As an upper bound to the quenched fraction, we assume that both elliptical and transitional morphologies correspond to quenched galaxies, while the lower bound for $f_{\rm quench}$ assumes only galaxies with elliptical morphologies are quenched. For each galaxy in the UNGC, which covers the entire Local Volume, we compute the distance to M31 and the Milky Way, adopting the lesser of the two as the host-centric distance. We then compute the quenched fraction, $f_{\rm quench}$, as a function of host-centric distance (see the grey shaded regions in Figures 4.2, 4.3, and 4.4). Our measured quenched fraction within the Local Volume is in good agreement with the observed fraction of early-type galaxies in the vicinity of other nearby massive hosts [**?**].

4.2.2 Simulations

The Local Group and its environs provide a unique laboratory for studying the details of how star formation in low-mass field and satellite galaxies is affected by the host environment. In order to take full advantage of this opportunity, a comparably specific suite of simulations is needed in order to understand both the details of the host environment and satellite population. That is, an unbiased comparison of observations in the Local Volume to galaxy formation and evolution theory requires simulations that span the entire Local Volume.

The Exploring the Local Volume in Simulations (ELVIS) project is a suite of cosmological

zoom-in dark matter-only simulations and is comprised of 24 Milky Way-like hosts as well as 12 Local Group-like pairs [**?**]. Each simulated Local Volume provides complete halo catalogs for $M_{\rm halo} > 2 \times 10^7$ M$_\odot$ and $V_{\rm max} > 8$ km s^{-1} within a high-resolution region spanning $2-5$ Mpc, so as to enable tracking of the orbital and accretion histories of all dark matter subhalos that could potentially host a M$_\star > 10^6$ M$_\odot$ dwarf galaxy. In addition, the ELVIS suite of simulations is uncontaminated by lower resolution particles out to at least 3 $R_{\rm vir}$ for each host, such that they reliably trace the properties of the nearby field dark matter halo population.

From ELVIS, we select dark matter halos and subhalos in the range $M_{\rm peak} = 5 \times 10^9 - 6 \times 10^{10}$ M$_\odot$, which corresponds to M$_\star = 10^6 - 10^8$ M$_\odot$ via the abundance matching (or stellar mass-halo mass) relation of **?**]. Varying the abundance matching prescription only has a minor affect on the typical infall times for subhalos in this mass regime and thus a negligible impact on our results [**?**]. In order to increase the precision at which we track subhalo accretion events, we interpolate, using a cubic spline, all of the dark matter halo properties in the ELVIS catalog, following **?**].

4.2.3 Quenching Models

The physical mechanisms that act upon a galaxy while in the vicinity of a more massive host are thought to suppress star formation through modification of the gas reservoir itself or by preventing the gas reservoir from replenishing its supply. However, there are many different potential mechanisms that can accomplish this and distinguishing which mechanism is operating in each satellite stellar mass regime can be challenging. In order to constrain the possible quenching mechanisms, our recent work has developed subhalo accretion-based models in N-body simulations that should capture the global properties of the quenching process and constrain the typical quenching timescale [**? ?**]. What follows is a brief description of

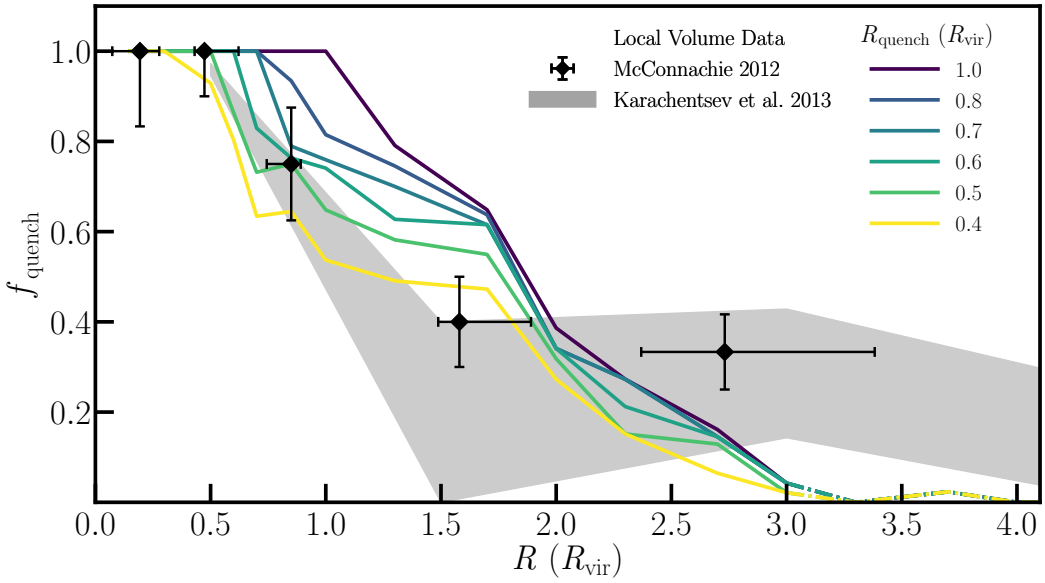

Figure 4.2: The quenched fraction as a function of host-centric distance for the $R_{\rm quench}$ model and Local Volume dwarfs. The black diamonds show the quenched fraction for our sample of Local Volume dwarfs (see Fig. 4.1) spanning five radial bins, with error bars on the host-centric distance corresponding to the $5^{\rm th}$ and $95^{\rm th}$ percentiles of the distribution in each respective bin and the error bars on $f_{\rm quench}$ denoting the 2σ uncertainty assuming binomial statistics. The grey shaded region illustrates a complementary measurement of the quenched fraction in the Local Volume determined using the UNGC. The upper bound is determined by assuming that both elliptical and transitional morphologies are quenched systems, while the lower bound assumes that only elliptical systems are quenched. Finally, the colored lines show the inferred quenched fraction in the ELVIS suite when varying the radius at which a subhalo is considered quenched, $R_{\rm quench}$. Beyond 3 $R_{\rm vir}$ the model lines are dot-dashed to illustrate the point at which some of the simulations in the ELVIS suite are contaminated by low resolution particles such that our modeling is less reliable. At $R < 2\ R_{\rm vir}$, there is excellent agreement between the observed quenched fraction and a model with $R_{\rm quench} = 0.5\ R_{\rm vir}$, such that all low-mass dwarfs within $\sim 2\ R_{\rm vir}$ of the Milky Way and M31 can be explained via environmental quenching. Beyond $\sim 2\ R_{\rm vir}$, the models cannot explain the observed quenched fraction such that these objects are likely self-quenching in the field.

both quenching models used in this work – see **?**] for a more detailed description.

$R_{\rm quench}$ Model

The first model that we examine is based on a "ram pressure-like" quenching scenario where quenching will only occur once a satellite reaches a sufficient host circumgalactic medium (CGM) density and/or a high enough velocity relative to the host frame-of-reference, such that the ram pressure experienced by a satellite is capable of disrupting its gas reservoir. Both the host CGM density and typical satellite velocity scale with host-centric distance, such that a model which includes a radial quenching dependence can broadly capture how these processes should affect the subhalo (i.e. satellite galaxy) population.

Within this model, any subhalo that crosses within the quenching radius ($R_{\rm quench}$) is instantaneously and permanently quenched, regardless of where the subhalo resides today. In contrast, those halos that never pass within the quenching radius remain star forming. By varying the quenching radius ($R_{\rm quench}$), in a manner similar to **?**], the model produces different quenched populations that can then be compared to the observed quenched fractions in the Local Volume, as shown in Figure 4.2. This model naturally leads to a quenched fraction of unity inside of the adopted quenching radius.

$\tau_{\rm quench}$ Model

The $\tau_{\rm quench}$ model assumes that quenching occurs at some time, $\tau_{\rm quench}$, after a dark matter halo crosses within the virial radius of the host (i.e. once it becomes a subhalo). In other words, the adopted quenching timescale ($\tau_{\rm quench}$) sets how long a dark matter halo must remain a subhalo before it is considered quenched. This model is able to approximate a "starvation-like" scenario, where the infalling satellite galaxy has been cut off from cosmic accretion and therefore will stop forming stars when it runs out of its current reservoir of fuel

(i.e. HI+H_2 gas). For relatively short quenching timescales, however, the model may also mimic suppression of star formation via ram-pressure stripping (e.g. where $\tau_{\rm quench}$ roughly follows the crossing time of the host system).

Within this model, all subhalos that remain inside the host dark matter halo at least as long as the quenching timescale are instantaneously and permanently quenched. Subhalos that enter and subsequently exit beyond the virial radius in less time than the quenching timescale remain star forming. Such halos are rare for short quenching timescales (< 2 Gyr), however, comprising $< 8\%$ of subhalos at $1 < R/R_{\rm vir} < 2$ within our mass range. As shown in Figure 4.3, by varying the quenching timescale, the $\tau_{\rm quench}$ model makes distinct predictions for how the quenched fraction depends on host-centric distance. Overall, a shorter timescale produces more quenched systems.

4.3 Results

For a wide range of quenching radii ($R_{\rm quench}$) and timescales ($\tau_{\rm quench}$), we apply the models described in §4.2.2 to the ELVIS subhalo populations. For each implementation of a given model, we measure the dwarf quenched fraction as a function of distance from the nearest host, extending to at least 3 $R_{\rm vir}$ (or $\gtrsim 0.9$ Mpc for these Milky Way-like systems). Figure 4.2 shows the results for the $R_{\rm quench}$ model, illustrating the quenched fraction, $f_{\rm quench}$, as a function of distance to the nearest host for values of $R_{\rm quench}$ ranging from 0.4 $R_{\rm vir}$ to 1 $R_{\rm vir}$. For comparison, the black diamonds show the observed quenched fraction in the Local Volume covering 5 bins in host-centric distance and the grey shaded region shows the UNGC quenched fraction as described in §4.2.1.

Within the satellite population ($R < R_{\rm vir}$), the observed quenched fraction is remarkably high ($f_{\rm quench} \sim 0.9$), so as to favor a quenching radius of 0.5 ± 0.1 $R_{\rm vir}$ [**?**]. For a quenching radius

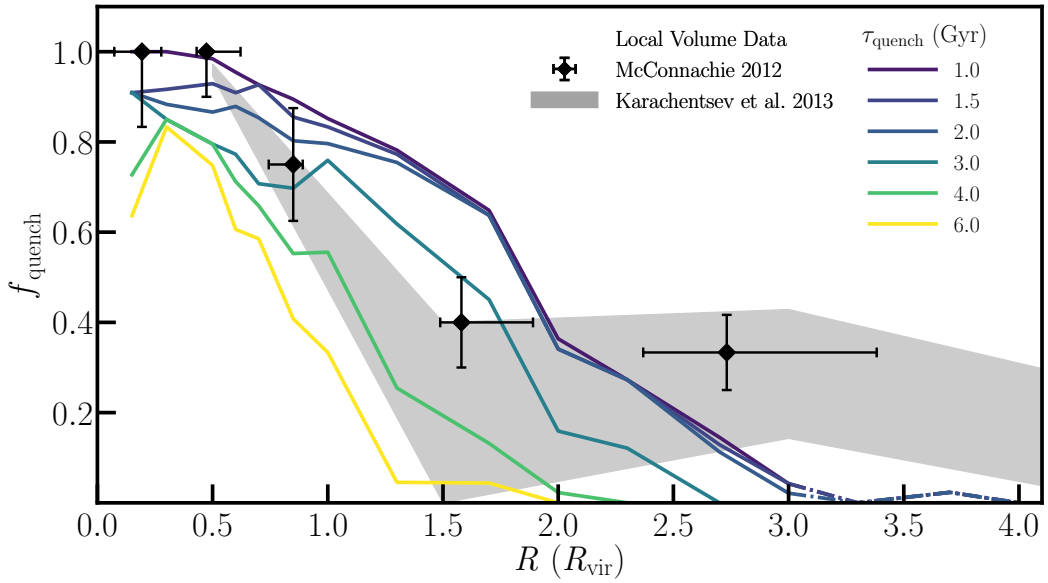

Figure 4.3: The quenched fraction as a function of host-centric distance for the $\tau_{\rm quench}$ model and Local Volume dwarfs. The black diamonds show the quenched fraction for our sample of Local Volume dwarfs (see Fig. 4.1) spanning five radial bins, with error bars on the host-centric distance corresponding to the $5^{\rm th}$ and $95^{\rm th}$ percentiles of the distribution in each respective bin and the error bars on $f_{\rm quench}$ denoting the 2σ uncertainty assuming binomial statistics. The grey shaded region illustrates a complementary measurement of the quenched fraction in the Local Volume determined using the UNGC, as detailed in Fig. 4.2. Finally, the colored lines show the inferred quenched fraction in the ELVIS suite when varying the quenching timescale from $\tau_{\rm quench} = 1 - 6$ Gyr. Beyond 3 $R_{\rm vir}$ the model lines are dot-dashed to illustrate the point at which some of the simulations in the ELVIS suite are contaminated by low resolution particles such that our modeling is less reliable. While the satellite quenched fraction in the Local Group favors $\tau_{\rm quench} = 1.5$ Gyr, such a short quenching timescale overproduces the observed quenched fraction at $1 < R/R_{\rm vir} < 2$ due to the contribution from backsplashing systems. Similar to the $R_{\rm quench}$ model, beyond ~ 2 $R_{\rm vir}$ the models cannot explain the observed quenched fraction such that these objects are likely self-quenching in the field.

on this scale, our $R_{\rm quench}$ model predicts a field quenched fraction of $f_{\rm quench} = 0.52 \pm 0.26$ at $1 < R/R_{\rm vir} < 2$ (see Fig. 4.2).[1] Overall, at $R < 2\ R_{\rm vir}$, our quenching model with $R_{\rm quench} = 0.5\ R_{\rm vir}$ is consistent with the observed field quenched fraction in the Local Volume, such that all passive systems at these distances can be explained through interactions with either the Milky Way or M31. Beyond $2\ R_{\rm vir}$, however, the backsplash fraction decreases dramatically such that the model predicts a quenched fraction $\lesssim 0.25$ for all quenching radii. At these distances from a massive host, the observed quenched fraction begins to exceed what the models predict by roughly a factor of two. The implications of this excess are discussed further in Section 4.4.

For the $\tau_{\rm quench}$ model, the quenched fraction of the Local Group satellite population (i.e. at $R < 1\ R_{\rm vir}$) is best reproduced by a quenching timescale of $\tau_{\rm quench} \sim 1.5 \pm 1$ Gyr [**?**]. As shown in Figure 4.3, this relatively short quenching timescale following infall yields a field quenched fraction of $f_{\rm quench} = 0.65 \pm 0.24$ within $1 < R/R_{\rm vir} < 2$, due to the large population of backsplash halos at that host-centric distance. Compared to observations of dwarf systems at similar distances in the Local Volume, this slightly overpredicts the fraction of quenched field galaxies. Meanwhile, at $R > 2\ R_{\rm vir}$, the $\tau_{\rm quench}$ models underpredict the fraction of passive systems found locally.

Ultimately, both the $R_{\rm quench}$ and $\tau_{\rm quench}$ models do not dramatically overpredict the field quenched fraction within the Local Volume. Instead, the models offer a potential explanation for a substantial number of the quenched dwarf galaxies that are observed outside of the virial radius of either the Milky Way or M31 today. Both models, however, do struggle to explain quenched systems beyond ~ 600 kpc from either of the Local Group hosts.

[1]The reported quenched fraction for both models is the mean quenched fraction in that distance range and the uncertainty is the 1σ scatter in the quenched fraction as measured individually for each ELVIS host.

4.4 Discussion

Recent work has shown that the vast majority of low-mass dwarf galaxies that reside in the field are star forming while a significant fraction that reside near a massive neighbor are quenched [e.g. **?**]. A likely consequence of this scenario is that all quenched dwarf galaxies observed in this mass regime ($M_\star \lesssim 10^9$ $M_\odot$) should have their star formation shut down via external, environmental processes. There have been many recent studies that test this picture under the assumption that the low-mass dwarf galaxy population in the Local Group is representative of the Universe at large [e.g. **? ? ? ? ? ?**].

However, the environmental-only quenching hypothesis for low-mass galaxies can be called into question in the Local Volume since there have been numerous quenched dwarf galaxies discovered beyond the virial radius of their most massive nearby neighbor. This has lead some studies to the conclusion that in-situ quenching of field dwarf galaxies is potentially occurring [**?**]. In this work, we have shown that our models of environmental quenching (i.e. quenching that only occurs inside $R_{\rm vir}$) can lead to a quenched fraction of ~ 0.5 beyond the virial radius but within 2 $R_{\rm vir}$. Beyond 2 $R_{\rm vir}$, it becomes increasingly difficult to explain the number of quenched galaxies through an interaction with either the Milky Way or M31.

4.4.1 Baryonic Effects on the Dark Matter Distribution

As shown by **?**], and more recently by **?**] and **?**], the baryonic component of the host system can substantially alter the final subhalo distribution inside the virial radius at $z = 0$ (relative to that found in a pure N-body simulation such as ELVIS). Due to tidal forces, subhalo destruction preferentially occurs in objects with early infall times and/or more radial orbits. As such, the distribution of subhalo infall times for a dark matter-only simulation (such as ELVIS) will be biased towards earlier cosmic times. Given our quenching models,

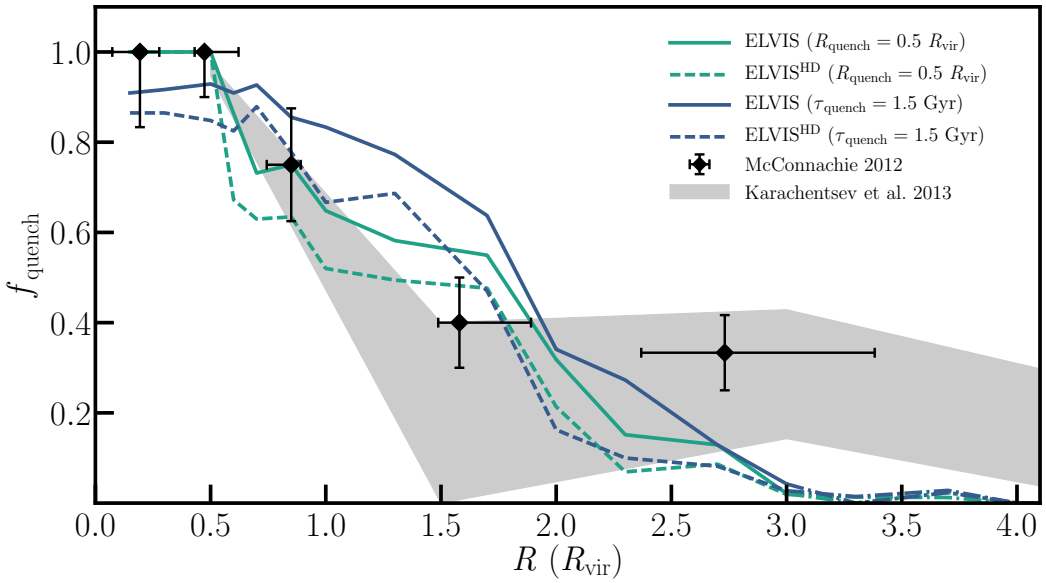

Figure 4.4: The quenched fraction as a function of host-centric distance for both the $\tau_{\rm quench}$ and $R_{\rm quench}$ models in comparison to the corresponding measurement in the Local Volume. The solid lines are the result of applying the quenching models to the ELVIS dark matter-only simulations, while the dashed lines show how our results change when we include the effects of tidal disruption by the host potential (ELVIS$^{\rm HD}$, see §4.4). The black diamonds and grey shaded region illustrate the measurements of the quenched fraction in the Local Volume as given in Fig. 4.2. As before, beyond 3 $R_{\rm vir}$ the model lines are dot-dashed to illustrate the point at which some of the simulations in the ELVIS suite are contaminated by low resolution particles. The inclusion of subhalo destruction due to tidal effects brings both models into better agreement with current observations, such that these models can fully explain the observed distribution of quenched dwarf galaxies within 2 $R_{\rm vir}$ of both the Milky Way and M31. For all of our modeling, quenched dwarf galaxies that currently reside beyond 2 $R_{\rm vir}$ cannot be fully explained via environmental quenching in either the Milky Way or M31 systems. Further emphasizing that self-quenching via star formation feedback is the likely quenching scenario in these objects.

which are directly connected to the accretion and orbital history of subhalos, this bias will skew the inferred quenched fractions as a function of host-centric distance.

In the $R_{\rm quench}$ model, the inclusion of the host system's baryonic potential will destroy many subhalos that plunge deep into the central regions of the host halo on highly radial orbits. Given that the majority of these systems will have pericentric passages within our adopted quenching radius, our model as applied to ELVIS is likely biased towards greater $f_{\rm quench}$ (see Fig. 4.2). Specifically, we have counted subhalos as "quenched" that would have been destroyed through interactions with a host baryonic potential, therefore overpredicting the quenched fraction within the Local Volume. Similarly, in the $\tau_{\rm quench}$ model as applied to ELVIS, we again overpredict the environmental quenched fraction, since the typical surviving subhalo in ELVIS spends more time inside the virial radius of the host. Subhalos accreted at early cosmic time, which are more likely to be tidally disrupted, are classified as quenched within our model, thereby over-counting the true number of quenched subhalos that survive to $z = 0$.

To demonstrate how subhalo destruction will affect the results presented in §4.3, we implement a correction to the ELVIS dark matter distributions that will broadly capture the tidal effects of the host. Figures 5 and A2 in **?**] show the fraction of subhalos that exist as a function of pericentric distance in two dark matter-only simulations of Milky Way-like host halos relative to the corresponding subhalo population in hydrodynamic simulations of the same hosts [using the FIRE model for star formation and feedback, **? ? ?**]. The ratio of subhalos in the dark matter-only versus hydro simulations roughly follows

$$N_{\rm DMO}/N_{\rm FIRE} = 40\, e^{-22\, d_{\rm peri}/{\rm kpc}}\ , \tag{4.1}$$

where $N_{\rm DMO}$ is the number of subhalos that survive to present day in the dark matter-only simulation, $N_{\rm FIRE}$ is the corresponding subhalo count for the hydrodynamic simulation, and

$d_{\rm peri}$ is the host-centric distance at pericenter in kpc. This radial dependence for subhalo disruption is supported by a larger number of dark matter-only simulations of Milky Way-like hosts run with an evolving disk potential (Kelley et al. in prep).

To mimic the disruption of subhalos in ELVIS, we adopt $(N_{\rm DMO}/N_{\rm FIRE})^{-1}$ as the likelihood that a subhalo survives as a function of pericentric distance. Beyond 50 kpc, we assume no subhalo destruction. Within ELVIS, we then randomly destroy subhalos as a function of their pericentric distance given this probability of survival. The results of this exercise can be seen in Figure 4.4 for the preferred values adopted in both the $R_{\rm quench}$ and $\tau_{\rm quench}$ models. For both models, we find a decrease in the quenched fraction relative to the same model applied to the dark matter-only simulations, with the difference being particularly strong for measurements of $f_{\rm quench}$ outside of $R_{\rm vir}$. Overall, the inclusion of tidal effects brings our model predictions into better agreement with the star-forming properties of dwarfs at $R < 2\ R_{\rm vir}$. At $R \gtrsim 2\ R_{\rm vir}$, however, tidal disruption has relatively little impact on the number of low-mass halos, with environmental processes unable to explain the suppression of star formation in the most distant dwarfs. Finally, it should be noted that the subhalo survival fraction given in Equation 4.1 is derived from a sample dominated by low-mass systems, such that our subhalo destruction model will likely overpredict the effect for the "classical" dwarfs. A conservative interpretation would be to treat the results of our tidal disruption models (as shown in Fig. 4.4) as a lower limit on the predicted quenched fraction in the Local Volume.

4.4.2 Quenched Dwarfs in the Field

As shown in §4.3, several of the passive dwarf systems in the local field population are potentially the product of environmental quenching mechanisms. Specifically, And XVIII, Phoenix, and Cetus currently reside within 2 $R_{\rm vir}$ of their nearest host, such that they

can potentially be explained with this model. **?**] measured the star formation histories (SFH) inferred from color-magnitude diagrams of resolved stars in Cetus and Phoenix [see also **?** **?** **?** **?**]. Both objects are consistent with a quenching event occurring roughly 2 Gyr ago. Additionally, **?**] inferred a relatively recent star formation event in And XVIII, approximately 1.5 Gyr ago. The quenched backsplash subhalos in our models that are currently located at similar distances from their most massive neighbor have a mean lookback time to infall of $t_{\rm infall} = 5.5 \pm 1.5$ Gyr. Assuming a quenching timescale ($\tau_{\rm quench}$) of ~ 2 Gyr, this suggests a quenching time of $\sim 2 - 5$ Gyr ago, consistent with the quenching times inferred from the measured SFHs of Cetus, Phoenix, and And XVIII. Lower-mass quenched systems within 2 $R_{\rm vir}$ [e.g. Eri II, **?** **?**] could have been influenced by environmental processes, however it is likely that reionization is at play in quenching the lowest-mass dwarfs independent of environment (**?** ; Wimberly et al. in prep).

At > 2 $R_{\rm vir}$, there are several passive dwarfs with $M_\star \sim 10^6 - 10^8$ $M_\odot$ in the Local Volume: Tucana, KK258, KKs3, and KKR 25 [**?** **?** **?** **?** **?** **?**]. These are very unlikely to have been quenched as a result of interaction with either the MW or M31. Instead, star formation in these systems was most likely suppressed via in-situ processes. One possibility is highly-efficient feedback, relative to the depth of the dark matter potential, that sufficiently disrupts the gas reservoir such that star formation is halted (if not completely shut down). Dwarf galaxies quenching in isolation (i.e. in the field), independent of environment, have been found in hydrodynamic simulations and can offer insight into the mechanisms responsible for shutting down star formation in these isolated dwarf galaxies [e.g. **?**].

4.5 Summary

Based on our analysis of quenching models applied to high-resolution N-body simulations, we show that the highly-efficient environmental quenching, required to suppress star formation

in the Local Group satellite population, does not overpredict the fraction of quenched systems in the local field. Within 2 $R_{\rm vir}$ of the Milky Way and M31, the passive population at $10^6 < \mathrm{M}_\star/\mathrm{M}_\odot < 10^8$ is consistent with being quenched by environmental processes. Moreover, beyond the Local Volume, we conclude that environmental mechanisms are likely at play in quenching a significant fraction of the low-mass ($\mathrm{M}_\star \lesssim 10^8$ $\mathrm{M}_\odot$), passive field systems observed in the local Universe [see also **?**]. Passive dwarfs at $R \gtrsim 2$ $R_{\rm vir}$, such as Tucana or KK25, are unlikely to have been quenched due to interaction with the Milky or M31. Instead, these systems may represent a tail of the star-forming field population, quenched by highly efficient feedback [e.g. **?** **?** **?**]. Altogether, our work adds further support to the model of satellite quenching outlined by **?** **?**], in which low-mass ($\mathrm{M}_\star \lesssim 10^8$ $\mathrm{M}_\odot$) satellites are rapidly quenched following infall onto a Milky Way-like host.

In conclusion, it should be noted that the broader impact of our work relies on the assumption that the star-forming properties of the Local Group and surrounding Local Volume are cosmologically representative [i.e. are not atypical, **?**]. Studies of low-mass satellites in other nearby systems, however, find a similarly high quenched fraction like that observed in the Local Group [e.g. **?**]. Moreover, by stacking photometric measurements of satellite populations surrounding a large sample of local Milky Way-like host systems in wide-field imaging datasets, Phillips et al. (in prep) measure a satellite quenched fraction of $f_{\rm quench} \sim 0.7$ at $\mathrm{M}_\star \sim 10^{6-9}$ $\mathrm{M}_\odot$ in broad agreement with that observed in the Local Group. On the other hand, observations of the NGC 4258 group find a significant number of blue, likely star-forming, satellites with $\mathrm{M}_\star < 10^8$ $\mathrm{M}_\odot$ [**?**]. In addition, recent work by **?**] to spectroscopically identify a large population of low-mass satellites orbiting Milky Way analogs finds very few passive systems, suggesting that the high satellite quenched fraction within the Local Group may be very atypical. Without question, more work remains to fully place the Milky Way (and more broadly the Local Group) in a cosmological context.

Chapter 5

Measuring the Quenching Timescales of Milky Way Satellites with *Gaia* Proper Motions

5.1 Introduction

Large surveys of the nearby Universe show that galaxies at (and below) the mass scale of the Magellanic clouds (10^6 $M_\odot \lesssim M_\star \lesssim 10^9$ $M_\odot$) are predominantly star forming in the field [**?** **?**]. This stands in stark contrast to the population of low-mass galaxies that currently reside near a more massive host system, where the fraction of systems that are no longer forming stars (i.e. "quenched") is significantly larger [**?** **?** **?**]. For dwarfs with $M_\star \lesssim 10^8$ $M_\odot$ in the Local Volume, this field-satellite dichotomy is very apparent, with satellites of the Milky Way (MW) and M31 being largely gas-poor, passive systems in contrast to the gas-rich, star-forming field population [e.g. **?** **?** **?**]. This clear distinction between the field and satellite populations strongly favors environmental processes as the dominant quenching mechanisms

in this low-mass regime [$M_\star \lesssim 10^8$ $M_\odot$, **? ? ? ? ? ? ?**]. At the very lowest mass scales (i.e. the regime of ultra-faint dwarfs), however, there is evidence for a transition in the dominant quenching mechanism from one associated with galaxy environment to one driven by reionization. The universally old stellar populations observed in the ultra-faint dwarfs (UFDs) suggest that star formation on the smallest galactic scales is suppressed at very early times and across all environments, marking a significant transition in the dominant quenching mechanism at the lowest masses [**? ?**].

Across all mass scales, some of the most powerful studies of satellite quenching have utilized measurements of satellite and field quenched fractions to infer the timescale upon which satellite quenching occurs following infall [e.g. **? ? ? ?**]. These studies point to a picture where quenching proceeds relatively slowly at high satellite masses, consistent with quenching via starvation [**?**]. Below some host-dependent critical mass scale, however, quenching is rapid, as stripping becomes increasingly efficient [**?**]. In defining this model of satellite quenching, simulations are commonly utilized to constrain the distribution of infall times for an observed sample of satellites. This statistical approach is required, as it is extremely difficult to infer the infall time for a significant fraction of the satellite population in even the most nearby groups and clusters. Moreover, in systems more distant than $\sim$ 1 Mpc, it is difficult to measure a precise star-formation history via spatially-resolved stellar photometry, even with the aid of imaging from the *Hubble Space Telescope* (*HST*). Within the LG, however, we are afforded the luxury of more detailed observations of the nearby satellite and field populations. This is particularly true with the release of *Gaia* Data Release 2 [DR2, **? ?**], which now enables an investigation of satellite quenching timescales (measured relative to infall) on an object-by-object basis. This offers a unique opportunity to test the results of large statistical analyses and our current physical picture of satellite quenching.

In this work, we aim to determine the quenching timescale and ultimately constrain the

potential mechanisms responsible for suppressing star formation in individual MW satellite galaxies. Utilizing the latest data products from *Gaia* DR2 [**?** **?**], we infer the cosmic time when each dwarf galaxy around the MW became a satellite (i.e. the infall time) through comparison to cosmological N-body simulations. In addition, we infer the quenching times for the MW satellites based on their published star-formation histories, as derived from *HST* imaging [**?** **?** **?**]. Finally, through comparison of the quenching times to the infall times, we will characterize the quenching timescales for each object and constrain the potential mechanisms responsible for quenching each MW satellite galaxy. In §**??**, we discuss our sample of local dwarfs and the methodology by which we measure the infall and quenching time for each system. Our primary results are presented in §4.3, followed by a discussion of how these results connect to physical models of satellite quenching in §4.4. Finally, we summarize our results and conclusions in §2.6. Where necessary, we adopt a ΛCDM cosmology with the following parameters: $\sigma_8 = 0.815$, $\Omega_m = 0.3121$, $\Omega_\Lambda = 0.6879$, $n_s = 0.9653$, and $h = 0.6751$ [**?**], consistent with the simulations used in this work.

Name	Distance	V_{3D}	V_r	e	t_{90}	t_{90}^{upper}	t_{90}^{lower}	t_{infall}	t_{infall}^{upper}	t_{infall}^{lower}
	(1)	(2)	(3)	(4)	(5)	(6)	(7)	(8)	(9)	(10)
Sgr_I	19.0	316.31	140.82	0.42	3.40	5.23	3.08	10.71	11.83	9.54
Tuc_III	23.0	241.56	-232.31	0.85	–	–	–	10.94	12.04	9.80
Hyd_I	26.0	413.93	-52.77	0.82	–	–	–	1.12	2.09	0.17
Dra_II	26.0	370.92	-156.38	0.57	–	–	–	9.71	11.09	6.01
Seg_1	28.0	233.12	116.48	0.37	–	–	–	10.78	11.84	9.73
Car_III	29.0	388.61	46.26	0.58	–	–	–	7.22	8.46	5.84
Seg_2	32.0	70.84	50.75	0.87	–	–	–	10.76	11.86	9.54
Ret_II	32.0	231.60	-102.07	0.32	–	–	–	10.99	12.08	9.81
Tri_II	36.0	335.57	-255.14	0.70	–	–	–	9.85	11.07	6.11
Car_II	37.0	356.19	203.77	0.64	–	–	–	7.86	11.17	6.28
U_Maj_II	38.0	258.39	-59.31	0.19	–	–	–	11.10	12.18	9.88
Boo_II	39.0	394.89	-47.85	0.68	–	–	–	1.02	1.99	0.06
Wil_1	43.0	123.08	18.05	0.53	–	–	–	10.79	11.86	9.67
ComBer_I	45.0	285.72	29.06	0.24	13.05	14.30	11.80	10.43	11.62	9.01
Tuc_II	54.0	285.79	-186.94	0.57	–	–	–	8.63	10.61	5.91
Boo_I	64.0	194.69	94.81	0.40	12.65	13.70	11.60	10.79	11.93	9.64
Dra_I	76.0	160.50	-88.41	0.53	10.15	11.68	7.66	10.82	12.01	9.38
U_Min_I	78.0	154.43	-71.46	0.50	9.07	10.67	5.79	10.82	12.01	9.38
Hor_I	80.0	198.80	-34.09	0.16	–	–	–	10.22	11.45	8.83
Scu_I	86.0	197.16	74.70	0.33	10.61	11.90	7.08	10.68	11.98	6.24
Sext_I	89.0	243.13	79.23	0.30	–	–	–	9.11	10.92	6.28
U_Maj_I	102.0	261.45	11.00	0.31	11.25	12.50	10.00	7.50	9.07	5.94
Aqu_II	105.0	294.26	43.31	0.50	–	–	–	1.43	2.40	0.48
Car_I	107.0	166.44	1.32	0.24	2.24	3.73	2.17	9.94	11.60	7.83
Gru_I	116.0	299.63	-202.68	0.75	–	–	–	0.76	1.78	0.00
Cra_II	116.0	115.54	-83.51	0.73	–	–	–	10.59	11.74	8.25
Her_I	126.0	211.67	150.74	0.59	11.85	13.20	10.50	6.52	10.43	5.40
Hyd_II	131.0	257.21	129.03	0.55	–	–	–	1.57	2.55	0.60
Cra_I	145.0	89.34	-13.19	0.65	–	–	–	10.34	11.63	8.73
Frn_I	149.0	159.71	-41.34	0.28	2.24	2.51	2.04	7.37	10.75	5.93
Leo_IV	155.0	355.66	12.79	0.98	12.15	13.60	10.70	10.26	11.45	8.81
CanVen_II	161.0	217.80	-92.93	0.40	12.70	14.30	11.10	1.18	2.13	0.21
Pis_II	182.0	390.20	-79.19	0.99	–	–	–	6.91	10.85	5.61
Leo_V	197.0	398.37	42.05	0.99	–	–	–	7.08	10.13	5.35
CanVen_I	218.0	142.78	83.72	0.55	8.32	9.46	6.31	7.25	8.66	5.82
Leo_II	236.0	118.81	16.05	0.43	6.41	7.16	5.81	7.48	9.07	5.83
Leo_I	257.0	183.48	168.25	0.85	1.68	1.89	1.62	2.45	3.45	1.44

Table 5.1: The properties of satellite galaxies of the Milky Way, as selected from **?**] and listed in order of increasing Galactocentric distance. (1) The distance from the center of the MW in kpc [**?**]. (2) The total velocity, in km s^{-1} in the Galactocentric frame-of-reference [**?**]. (3) The radial velocity, in km s^{-1} in the Galactocentric frame-of-reference [**?**]. (4) The eccentricity, e, based on the "heavy" MW mass used in **?**]. (5) The quenching time, t_{90}, in Gyr, inferred from the SFHs by adopting the lookback time at which the dwarf galaxy formed 90% of its current stellar mass [**?** **?**]. (6,7) The 1σ bounds on the quenching time, in Gyr, inferred from the SFHs by adopting the lookback-time at which the 1σ bounds on the SFH crossed the 90% threshold. (8) The infall time, in Gyr, from matching the observed

Chapter 6

Conclusion

Awesome conclusion...astrophysics is still cool!

Maybe I helped make is cooler...unlikely...#impostersyndrom

Wrap it up!!